

**APPENDICES**

ลิขสิทธิ์มหาวิทยาลัยเชียงใหม่

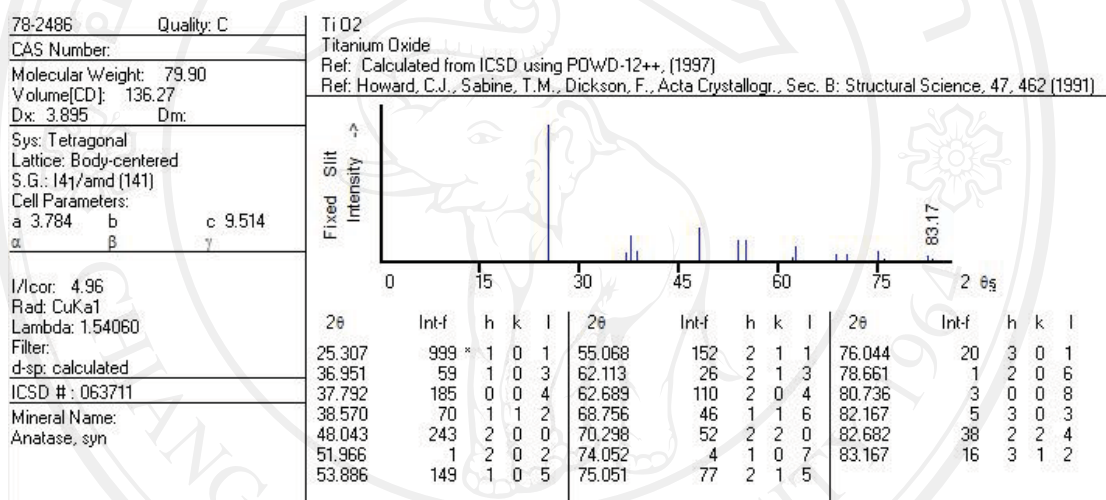
Copyright© by Chiang Mai University

All rights reserved

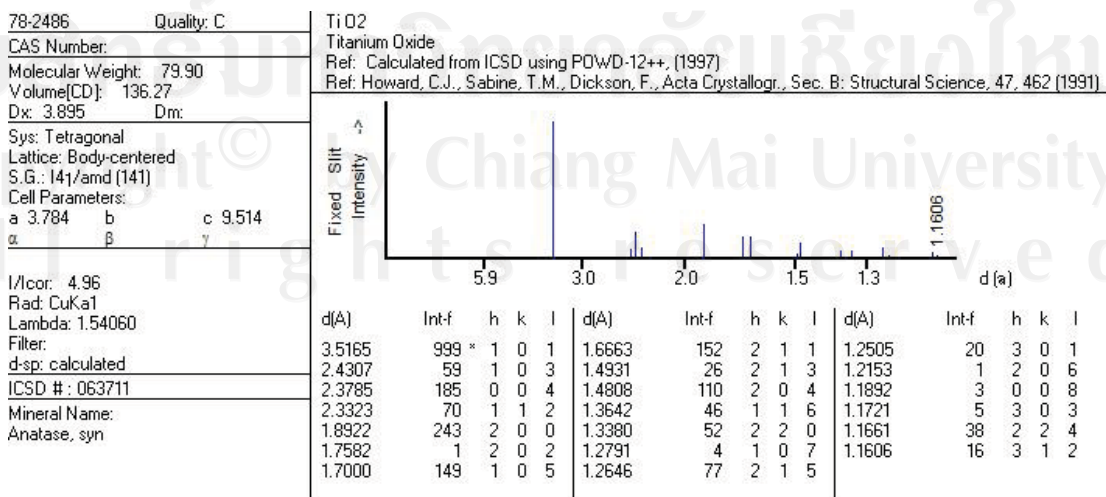
## APPENDIX A

### 1. JCPDS No. 78-2486 (Anatase TiO<sub>2</sub>)

#### 2 Theta

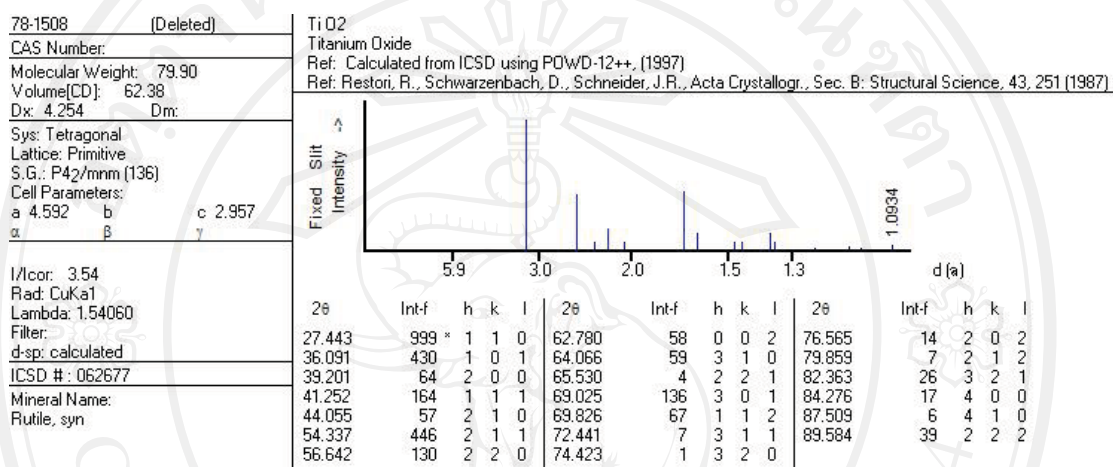


#### D Spacing (D)

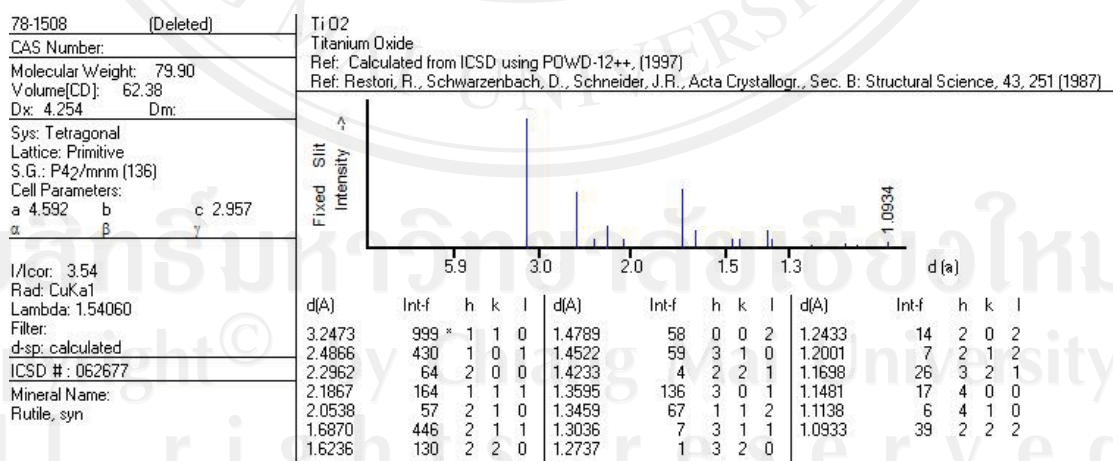


2. JCPDS No. 78-1508 (Rutile TiO<sub>2</sub>)

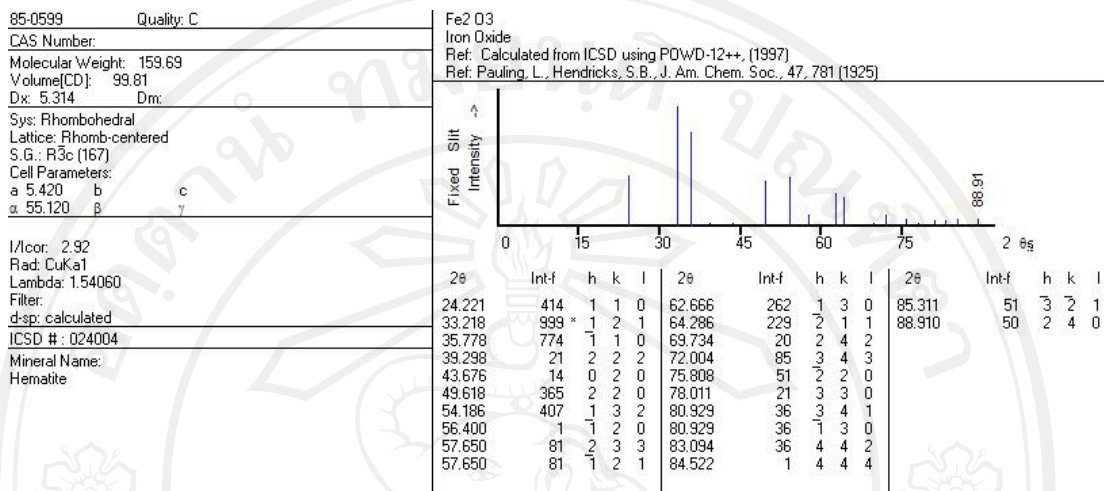
## 2 Theta



## D spacing (D)



### 3. JCPDS No. 89-0599 (Hematite $\alpha$ -Fe<sub>2</sub>O<sub>3</sub>)



ลิขสิทธิ์มหาวิทยาลัยเชียงใหม่  
 Copyright© by Chiang Mai University  
 All rights reserved



**APPENDIX B**

**International Publication**

ลิขสิทธิ์มหาวิทยาลัยเชียงใหม่

Copyright© by Chiang Mai University

All rights reserved



## Photocatalytic property of colloidal TiO<sub>2</sub> nanoparticles prepared by sparking process

W. Thongsuwan, T. Kumpika, P. Singjai \*

*Nanomaterials Research Unit, Department of Physics, Faculty of Science, Chiang Mai University, Chiang Mai 50200, Thailand*

Received 24 May 2007; received in revised form 24 September 2007; accepted 5 October 2007

Available online 12 October 2007

### Abstract

Titanium oxide nanoparticles (NPs) were successfully prepared by sparking off two titanium tips into water for 1–5 h. The nanoparticle-dispersed water was obtained for further characterization. The transmission electron microscopy result shows that the particle size is in the range of 1–5 nm. The electron diffraction patterns and Raman spectra reveal that the as-prepared and the annealed samples at 250 °C are the anatase phase. However, the anatase–rutile phase transformation was observed from the samples at annealing temperature as low as 500 °C. The result of methylene blue-decoloration testing under sunbath suggests that the NPs have good photocatalytic property.

© 2007 Elsevier B.V. All rights reserved.

PACS: 61.46.Df; 81.07.-b; 81.16.-c

Keywords: Spark; Titanium oxide; Nanoparticles; Methylene blue

### 1. Introduction

Titanium oxide nanoparticles in the anatase phase have been found active for photocatalytic degradation of inorganic or organic compounds in the treatment of wastewater as well as in solar cell [1–3]. The synthesis of TiO<sub>2</sub> NPs is an important issue for utilizing in many applications [4–6]. Therefore, many methods have been extensively developed, such as flame spray pyrolysis [7], hydrolysis [8], chemical reduction [9], sol–gel [10] and gas matrix-assisted pulsed laser evaporation [11]. However, in many cases a hazardous byproduct formation is unavoidable when a titanium compound, such as TiCl<sub>4</sub> is used as a precursor.

As is well known, there are three naturally occurring phases: anatase, brookite and rutile phases in which the anatase phase is most commonly utilized for photocatalytic activity [12]. It is also known that surface properties of TiO<sub>2</sub> NPs including their particle sizes and specific surface

area obviously influence the photocatalytic activities [13–16]. Therefore, many research interests have recently developed alternative ways to prepare anatase TiO<sub>2</sub> NPs with high specific surface area. In this work, colloidal TiO<sub>2</sub> NPs were prepared by a novel, simple and clean method as well as an environmental friendly means. Structural, optical characterization and photocatalytic property of the obtained NPs were investigated.

### 2. Experimental details

The sparking off two sharp titanium tips for preparation of TiO<sub>2</sub> NPs were done in a glass bottle filled with 10 ml distilled water. The two sharp titanium tips (∅ 0.25 mm, purity 99.5%, Advent Research Material Ltd.) were prepared by cutting with pliers and placed horizontally at 3 mm spacing (*d*) and 2 mm above a water level (*h*). As schematically depicted in Fig. 1, the power supply for a sparking voltage of 3 kV with a limited current of 3 mA was connected to the apparatus. The NPs were then continuously deposited into the water by the sparking for 1–5 h.

\* Corresponding author. Tel.: +66 53 941922x610; fax: +66 53 892271.  
E-mail address: [singjai@chiangmai.ac.th](mailto:singjai@chiangmai.ac.th) (P. Singjai).

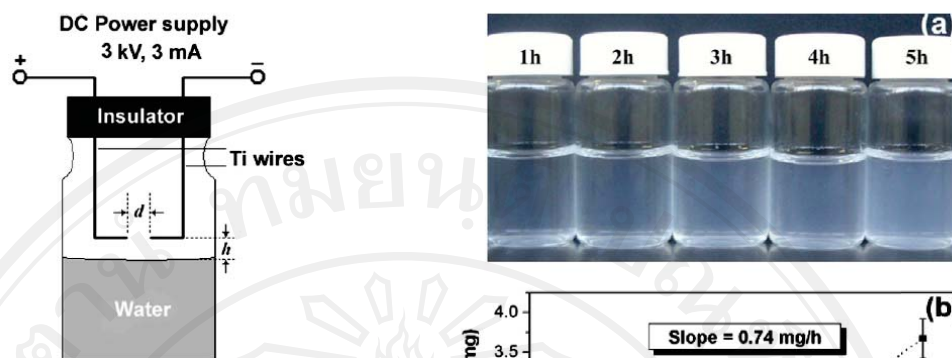


Fig. 1. Schematic diagram of the sparking apparatus.

The NP-dispersed water was obtained and separated for further characterizations.

TiO<sub>2</sub> NPs were deposited on quartz substrates ( $1 \times 10 \times 10 \text{ mm}^3$ ) by two drops of the NP-dispersed water. The deposited samples were annealed at 250 and 500 °C in air for 1 h. The morphologies were observed by SEM (JEOL JSM-6335F). The particle sizes and structural properties of the NPs were investigated by TEM (JEOL JEM-2010) and Raman spectrometer with a 514.5 nm argon ion laser at room temperature (JOBIN YVON HORIBA T64000). The optical properties were measured in the visible region by UV–vis spectrophotometer (Perkin–Elmer Instruments). The transmittance spectra were analyzed using the modified envelope method, which allows the absorption coefficient to be determined.

The photocatalytic properties of the obtained colloidal TiO<sub>2</sub> NPs at 1.0 vol% of 0.01 mM methylene blue (MB) solution (Ajax Finechem) were investigated by measuring the photocatalytic decomposition under sunbath for 1 h. Variation in the concentration of MB was monitored by UV–vis spectroscopy (Perkin–Elmer Instruments).

### 3. Results and discussion

Fig. 2a shows a photograph of TiO<sub>2</sub> NPs which were prepared for 1–5 h in glass bottles filled with 10 ml of distilled water. It is noted that concentration of the NPs linearly increased with increasing the sparking time at the rate of 0.74 mg/h, as shown in Fig. 2b. The primary particle sizes and their size distribution of the as-prepared sample at the sparking time of 1 h were in the range of 1–5 nm, as shown in Figs. 3a and 4, respectively. However, at the longer sparking time of 5 h (Fig. 3b), density and agglomeration of the particles increased whereas the primary particle sizes were in the same range. The similar SAED patterns of samples for sparking times of 1 and 5 h (insets of Fig. 3a and b) have shown the five main sharp diffraction rings of (101), (004), (200), (211) and (204) planes which corresponded to the anatase (tetragonal) phase [17]. SEM images in Fig. 5a, b and c show the as-prepared TiO<sub>2</sub>

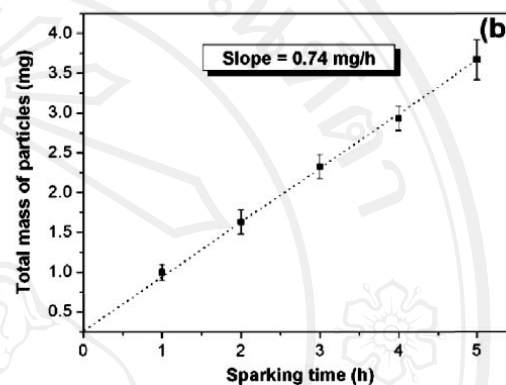


Fig. 2. (a) Photograph of TiO<sub>2</sub> NPs deposited into 10 ml of distilled water at various sparking time, and (b) total mass of the NPs vs. the sparking time, obtained by hot-plate drying and weighing in a small aluminum-foil crucible.

NPs deposited on quartz substrates by the two drops of NP-dispersed water and the annealed samples at 250 and 500 °C for 1 h in air, respectively. It is noted that the particle size of the samples increased with increasing the annealing temperature [18,19].

Fig. 6a shows the Raman spectra of the as-prepared sample and the annealed samples at 250 and 500 °C. The peaks corresponded to the anatase and rutile phases are marked. It is noted that the anatase peaks at 148, 200, 405, 519 and 638  $\text{cm}^{-1}$  increased with increasing the annealing temperature. This result is in good agreement with the previous report that different TiO<sub>2</sub> crystalline structures were obtained from different annealing temperatures [20]. However, weak rutile peaks at 448 and 612  $\text{cm}^{-1}$  were also observed from the annealed samples at 500 °C. Interestingly, the anatase–rutile phase transformation temperature in this work is lower than the reports of Xia and co-workers and Kim and co-workers [21,22]. It is attributed that the high specific surface area of the smaller size anatase TiO<sub>2</sub> NPs transformed to the rutile phase at the lower temperature, as compared in Table 1 and Fig. 7.

Fig. 6b shows a relative intensity, a peak-center and a full width at half maximum (FWHM) of the strong anatase peak at approximately 148  $\text{cm}^{-1}$ . It is known that the anatase peaks strongly depend on the annealing temperature

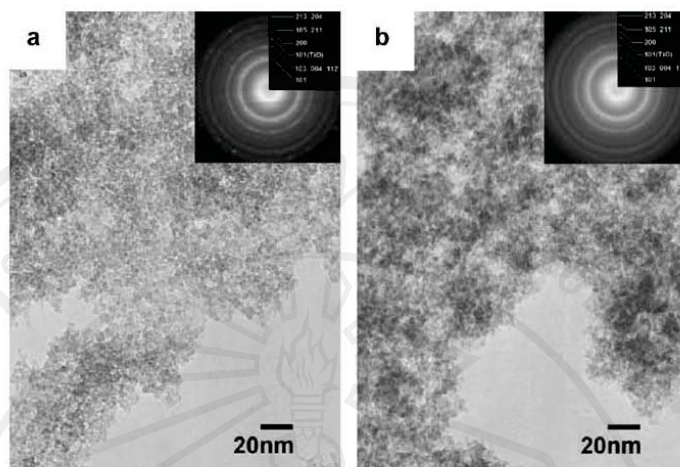


Fig. 3. TEM images and their corresponding SAED patterns of the as-deposited NPs at sparking times of (a) 1 h, and (b) 5 h.

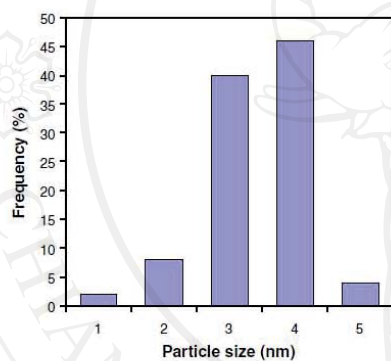


Fig. 4. Size distribution of the as-prepared  $\text{TiO}_2$  NPs.

[20]. As apparently seen, the weak peak and the stronger peaks were observed from the as-prepared sample and the annealed samples, respectively. Under closer examination, the FWHM change and the peak-center shift are in good agreement with the report of Zhang and co-workers, as shown in Fig. 6c. These results were attributed to phonon confinement and non-stoichiometry effects [23].

The UV–vis transmission spectra of the samples prepared as for Raman spectra are shown in Fig. 8. The light transmittance ( $T$ ) of approximately 90% was slightly changed within the wavelength range from 650 to 400 nm and abruptly decreased to less than 5% from 395 to 350 nm. The result has shown that the photon energy absorption fairly corresponds to  $\text{TiO}_2$  energy gap [24]. The inset of Fig. 8 shows  $(\alpha h\nu)^2$  plotted as a function of the photon energy ( $h\nu$ ), where  $\alpha$  is the absorption coefficient;  $\alpha = \ln(1/T)$  [25]. By assuming that the electron transition between the conduction and valence bands was a direct

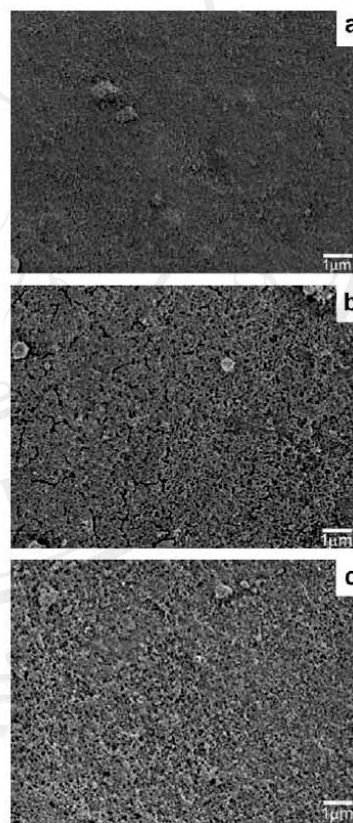


Fig. 5. SEM images of (a) the as-deposited NPs on quartz substrate by two drops of the NP-dispersed water, (b) the annealed sample at 250 and (c) 500 °C.



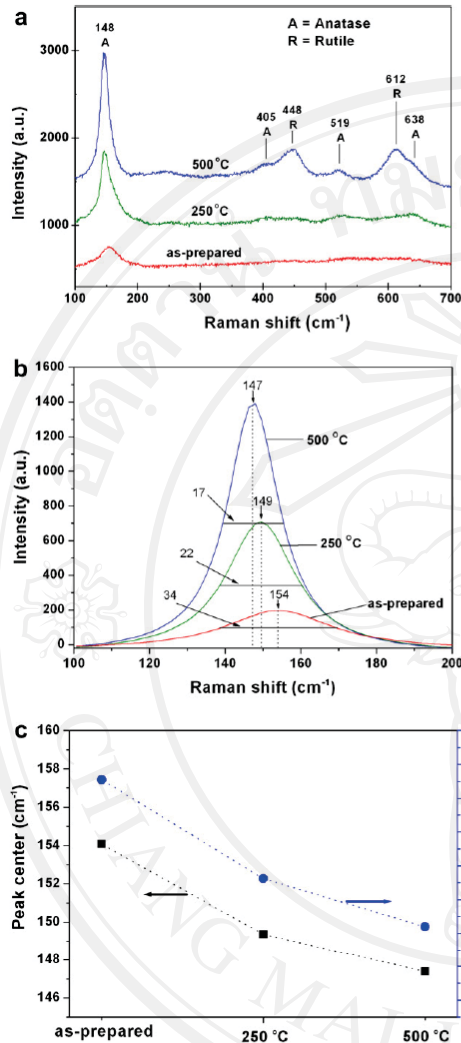


Fig. 6. (a) Raman spectra, (b) the main anatase peak and (c) plot of main anatase peak and its FWHM against the as-prepared NPs, the annealed samples at 250 and 500 °C.

Table 1  
Comparison of anatase-rutile phase transformation temperature at various particle sizes of TiO<sub>2</sub> NPs

Result from	Mean diameter (nm)	Transformation temperature (°C)
This work	3	500
Kim et al. [22]	11	650
	21	750
Xia et al. [21]	17	650
	25	750
	45	950

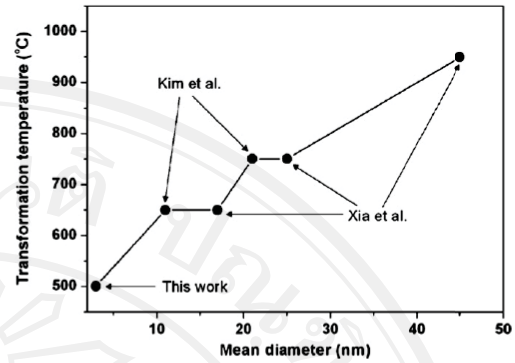


Fig. 7. Plot of the phase transformation temperature against the mean particle size of TiO<sub>2</sub> NPs.

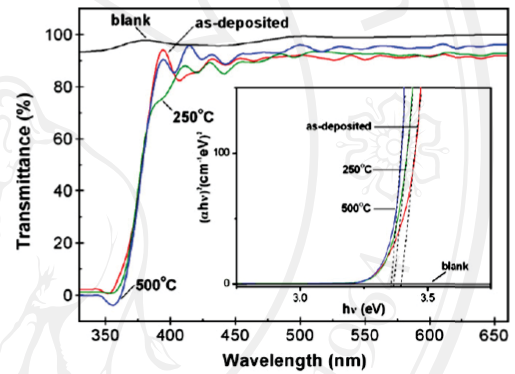


Fig. 8. Plots of optical transmittance against the wavelength of the as-deposited NPs and the annealed samples at 250 and 500 °C for 1 h. Inset: the variation of  $(\alpha h\nu)^2$  vs.  $h\nu$  of the thin films for estimation of the  $E_g$ .

transition, the energy gap was estimated by extrapolating linearly to  $(\alpha h\nu)^2 = 0$  [26]. As the result, the energy gaps of the as-prepared sample, the annealed samples at 250 and 500 °C were estimated to be 3.40, 3.36 and 3.35 eV, respectively. The obtained energy gaps were slightly blue-shifted from bulk TiO<sub>2</sub>, which were reported to be 3.2 eV for anatase and 3.0 eV for rutile [27]. Such the result was attributed to the phonon confinement effect, crystalline defects and/or oxygen defects [28].

Degradation of MB by colloidal TiO<sub>2</sub> NPs for various sparking times under sunbath for 1 h is shown in Fig. 9a. As we expected, the absorption peaks occurred commonly at 665 and 292 nm [29–31] and the peaks gradually decreased with increasing of the sparking time from 1 to 5 h. In other words, the degradation of MB gradually increased with increasing concentration of the NPs. Moreover, fundamental photocatalytic activity of TiO<sub>2</sub> NPs was investigated by a calibration using UV–vis absorption of

Copyright © by Chia...  
All rights reserved

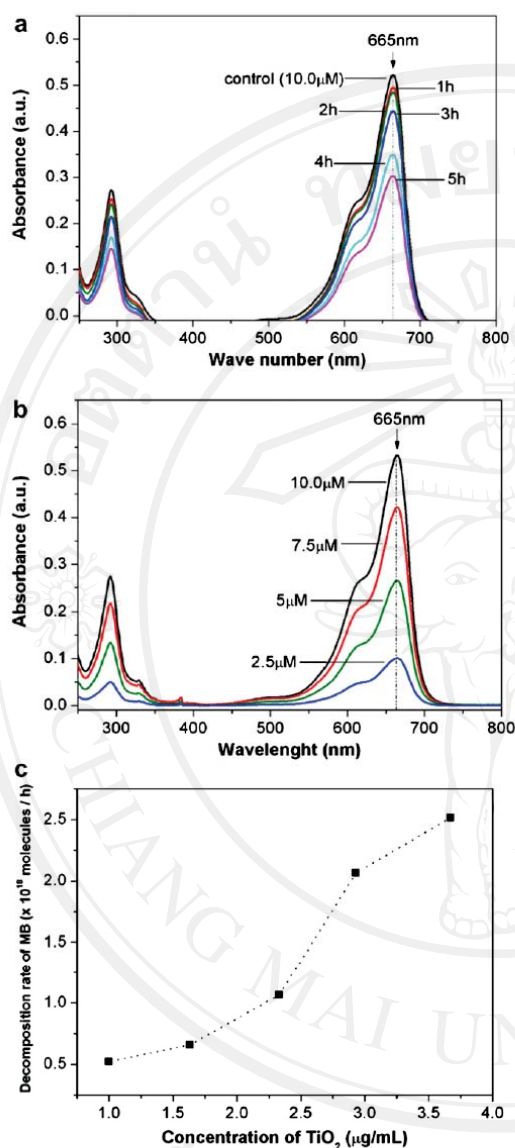


Fig. 9. UV-vis adsorption spectra of (a) 10  $\mu\text{M}$  MB solution containing the as-prepared  $\text{TiO}_2$  NPs at the various sparking times under sunbath for 1 h, and (b) dilute MB solution at the concentration range of 10–2.5  $\mu\text{M}$  without  $\text{TiO}_2$  NPs. (c) The decomposition rate of MB vs. the concentration of  $\text{TiO}_2$  NPs.

dilute MB solution without  $\text{TiO}_2$  NPs, as shown in Fig. 9b, and the obtained mass of  $\text{TiO}_2$  NPs, as shown in Fig. 2b. It was found that the decomposition rate of MB at 10  $\mu\text{M}$  were in the range of  $0.5\text{--}2.5 \times 10^{18}$  mol/h for the solution

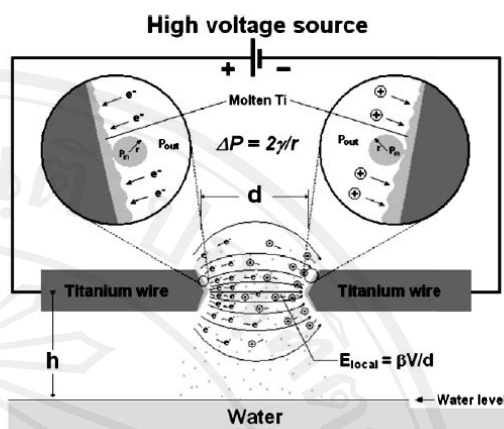


Fig. 10. Schematic diagram of the nucleation mechanism of the NPs prepared by the sparking off two Ti sharp tips.

containing  $\text{TiO}_2$  NPs at the dilute concentration range of 1.0–3.67  $\mu\text{g/mL}$ , as shown in Fig. 9c.

As shown in the TEM images of Fig. 3a and b, the sparking time affected not only the concentration of  $\text{TiO}_2$  NPs but also the agglomeration to form bigger secondary particles which reduced the specific surface area and hence, the photocatalytic activity. However,  $\text{TiO}_2$  NP concentration used in this work was diluted, therefore the decomposition rate of MB apparently increased with increasing the catalyst (Fig. 9c). The effect of agglomeration on the reduction of photocatalytic activity is probably dominant at the higher concentration of  $\text{TiO}_2$  NPs.

The nucleation mechanism of NPs prepared by the sparking process was primarily discussed in our previous paper [32]. However, in the case of two Ti sharp tips, the high temperature and pressure on molten Ti at the two tip surfaces were generated by the bombardment of both electrons and ions, as shown in Fig. 10.

#### 4. Conclusion

In summary, the anatase  $\text{TiO}_2$  NPs were successfully prepared by the sparking off two titanium tips into water. The obtained particle size is as small as 1–5 nm. The methylene blue-decoloration testing under sunbath suggests that the colloidal  $\text{TiO}_2$  NPs prepared by this present work have good photocatalytic property. Thus, we suggest that the sparking process can be used to prepare many other colloidal metal/metal-oxide NPs.

#### Acknowledgements

This work was supported by the Thailand Research Fund and the Commission on Higher Education. The authors would like to thank Mr. Ekkapong Kuntarak for

his help in Raman spectroscopy measurements. W. Thongsuwan is grateful for his PhD scholarship from the Commission on Higher Education.

#### References

- [1] H. Choi, E. Stathatos, D.D. Dionysiou, *Desalination* 202 (2007) 199.
- [2] Z. Guo, R. Ma, G. Li, *Chem. Eng. J.* 119 (2006) 55.
- [3] Y. Tachibana, H.Y. Akiyama, S. Kuwabata, *Sol. Energy Mat. Sol. C* 91 (2007) 201.
- [4] H.C. Huang, G.L. Huang, H.L. Chen, Y.D. Lee, *Thin Solid Films* 511–512 (2006) 203.
- [5] M. Pal, T. Sasaki, N. Koshizaki, *Scripta Mater.* 44 (2001) 1817.
- [6] J.H. Park, M.A. Lee, B.J. Park, H.J. Choi, *Curr. Appl. Phys.* 7 (2007) 349.
- [7] A. Telesi, S.E. Pratsinis, K. Kalyanasundaram, P.I. Gouma, *Sensor. Actuat. B* 119 (2006) 683.
- [8] S. Mahshid, M. Askari, M.S. Ghamsari, *J. Mater. Process. Tech.* 189 (2007) 296.
- [9] K.D. Kim, D.N. Han, J.B. Lee, H.T. Kim, *Scripta Mater.* 54 (2006) 143.
- [10] X. Li, X. Quan, C. Kutal, *Scripta Mater.* 50 (2004) 499.
- [11] A.P. Caricato, M.G. Manera, M. Martino, R. Rella, F. Romano, J. Spadavecchia, T. Tunno, D. Valerini, *Appl. Surf. Sci.* 253 (2007) 6471.
- [12] Y. Sun, A. Li, M. Qi, L. Zhang, X. Yao, *Mater. Sci. Eng. B* 86 (2001) 185.
- [13] J.C. Yu, J.G. Yu, J.C. Zhao, *Appl. Catal. B* 36 (2002) 31.
- [14] C.P. Siby, S. Rajesh Kumar, P. Mukundan, K.G.K. Warriar, *Chem. Mater.* 14 (2002) 2876.
- [15] J.C. Yu, J.G. Yu, W.K. Ho, Z.T. Jiang, L.Z. Zhang, *Chem. Mater.* 14 (2002) 3808.
- [16] V. Subramanian, E.E. Wolf, P.V. Kamat, *J. Am. Chem. Soc.* 126 (2004) 4943.
- [17] S. Park, E. DiMasi, Y.-I. Kim, W. Han, P.M. Woodward, T. Vogt, *Thin Solid Films* 515 (2006) 1250.
- [18] C. Legrand-Buscema, C. Malibert, S. Bach, *Thin Solid Films* 418 (2002) 79.
- [19] S. Karuppachamy, M. Iwasaki, H. Minoura, *Appl. Surf. Sci.* 253 (2006) 2924.
- [20] M.L. Hitchman, F. Tian, *J. Electroanal. Chem.* 538–539 (2002) 165.
- [21] B. Xia, H. Huang, Y. Xie, *Mater. Sci. Eng. B* 57 (1999) 150.
- [22] C.S. Kim, I.M. Kwon, B.K. Moon, J.H. Jeong, B.C. Choi, J.H. Kim, H. Choi, S.S. Yi, D.H. Yoo, K.S. Hong, J.H. Park, H.S. Lee, *Mater. Sci. Eng. C* 27 (2007) 1343.
- [23] W.F. Zhang, Y.L. He, M.S. Zhang, Z. Yin, Q. Chen, *J. Phys. D: Appl. Phys.* 33 (2000) 912.
- [24] H.P. Deshmukh, P.S. Shinde, P.S. Patil, *Mater. Sci. Eng. B* 130 (2006) 220.
- [25] Q. Wang, G. Wang, J. Jie, X. Han, B. Xu, J.G. Hou, *Thin Solid Films* 492 (2005) 61.
- [26] T. Toyoda, H. Kawano, Q. Shen, A. Kotera, M. Ohmori, *J. Appl. Phys.* 39 (2000) 3160.
- [27] S.D. Mo, W.Y. Ching, *Phys. Rev. B* 51 (1995) 13023.
- [28] H.C. Ong, A.X.E. Zhu, G.T. Du, *Appl. Phys. Lett.* 80 (2002) 941.
- [29] A. Mills, J. Wang, *J. Photochem. Photobiol. A* 127 (1999) 123.
- [30] T. Zhang, T. Oyama, A. Aoshima, H. Hidaka, J. Zhao, N. Serpone, *J. Photochem. Photobiol. A* 140 (2001) 163.
- [31] K.T. Byun, H.Y. Kwak, *J. Photochem. Photobiol. A* 175 (2005) 45.
- [32] T. Kumpika, W. Thongsuwan, P. Singjai, *Surf. Interface Anal.* 39 (2007) 58.

## Antibacterial activity of TiO<sub>2</sub> nanoparticles prepared by sparking process

W. Thongsuwan<sup>a</sup>, T. Kumpika<sup>a</sup>, P. Thongmanee<sup>b</sup>, S. Bovonsombut<sup>b</sup> and P. Singjai<sup>a,\*</sup>

<sup>a</sup>Nanomaterials Research Unit, Department of Physics, Faculty of Science,  
Chiang Mai University, Chiang Mai 50200, Thailand

<sup>b</sup>Department of Biology, Faculty of Science, Chiang Mai University,  
Chiang Mai 50200, Thailand

\*Corresponding author. *Tel:* +66 53 941922 ext. 610, *Fax:* +66 53 892271

*E-mail address:* singjai@chiangmai.ac.th (P. Singjai)

### Abstract

Antibacterial properties of TiO<sub>2</sub> nanoparticles (NPs) prepared by a sparking process against *Escherichia coli* (*E.coli*) were examined by the so-called antibacterial-drop test. The results show that a survival rate of *E.coli* supplemented with colloidal TiO<sub>2</sub> NPs under UV light abruptly decreased with increasing the reaction time and highly decreased in the dark. The scanning electron microscopy result shows that most of the treated *E.coli* cell walls were deteriorated by the photocatalytic activity. Moreover, the transmission electron microscopy result confirms that the NPs migrated through the cell wall to inside the bacterial cells causing the structural changes, the deterioration and finally, the cell death.

*Keyword:* TiO<sub>2</sub> ; Nanoparticles ; photocatalysis ; Antibacterials ; *E.coli*

### 1. Introduction

Photocatalytic properties of TiO<sub>2</sub> nanostructures have been widely used for environmental applications, such as photocatalytic degradations of various organic contaminants in wastewater and air [1,2] including antibacterial applications [3,4]. The interaction between the UV light and TiO<sub>2</sub> produces two highly reactive oxygen species: superoxide anion ( $\bullet O_2^-$ ) and hydroxyl radicals ( $\bullet OH$ ) which are responsible for organic decomposition and bacterial inactivation [5].

TiO<sub>2</sub> NPs are relatively inexpensive, non-toxic and photochemically stable [6,7]. Thus, they are generally used as a photocatalytic material. Moreover, their high specific

surface area of the NPs is very crucial to maximize the reaction sites as well as charge carriers ( $e^-$  and  $h^+$ ) have to be utilized properly to improve their ability to initiate surface reactions [8,9].

As reported in our previous paper [10], a novel method to prepare  $TiO_2$  NPs by the sparking process was described. The result of methylene blue decomposition testing under sunbath shows that the NPs have a good photocatalytic activity. In this paper,  $TiO_2$  NPs prepared by this novel process were used as a photocatalyst for antibacterial activity against the Gram negative *E.coli* by using the antibacterial-drop test [11,12]. Bacterial morphologies before and after treatment with the NPs were observed. Moreover, the antibacterial activity and its mechanism at the various reaction times were discussed.

## 2. Experimental details

*E.coli* TISTR 527 was used selected as the common indicator bacteria [13,14]. Luria broth (LB) medium (Miller, Cat. No. C6011) was prepared by mixing of 10 g casein peptone, 10 g sodium chloride, 5 g yeast and 1 L deionized water before 15 g agar was added to produce LB agar which was autoclaved at 121 °C for 15 min. *E.coli* standard was then cultured onto LB agar and incubated at 37 °C for 24 h. The cultured bacterial cells were diluted to approximately  $10^8$  colony forming unit per milliliter (CFU/mL) in order to comparison with standard 0.5 Mc Farland.

The process of bactericidal on Gram-negative bacterial was prepared as shown in Fig. 1. The experiment was started by using 0.2 mL of diluted *E.coli* supplemented with 0.2 mL of colloidal  $TiO_2$  NPs (1-5 nm in diameter and concentration of 0.25 mg/mL) prepared by the sparking process [10]. The samples were then kept in the dark and under UV light for 0, 1, 2 and 4 h. Each condition was diluted by 5 mL of phosphate buffer, dropped of 10  $\mu$ L onto agar plate and incubated at 37 °C. The colony counts were taken after 24 h of the incubation. The morphology and microstructure of bacteria cells were characterized by scanning electron microscopy (SEM, JEOL JSM-6335F) and transmission electron microscopy (TEM, JEOL JEM-2010) which the sections were cut at a thickness of 90 nm by a microtome.

### 3. Results and Discussion

Fig. 2a, b and c show photographs of the samples which were kept under UV light without the NPs, supplemented with the NPs in the dark and under UV light for various lengths of time, respectively. The survival rate of *E.coli* can be estimated by count the number of colony from Fig. 2, as shown in Fig. 3. The survival rate of the sample kept under UV light without NPs gradually decreased from 100 % to 67, 60 and 34 % at the reaction times of 0, 1, 2 and 4 h, respectively. In comparison with the rate of the sample supplemented with NPs in the dark was highly decreased from 24 to 20, 14 and 4 %. Interestingly, the survival rate of the sample supplement with NPs under UV light was abruptly decreased from 20 to almost 0 % within 1 h. This result is in good agreement with some previous works that the UV light itself can be used to treat the *E.coli* [3-5,15,16]. It is clearly seen that the antibacterial effect of the NPs themselves is better than that of the UV light whereas that of both factors together is the best.

Fig. 4 shows SEM images of the morphologies of *E.coli* cells before (a) and after treated with NPs under UV light for 4 h. The results show that the structure of the treated cells was damaged due to the effect of photocatalytic reaction took place on the surface of NPs which interact with the intact cells. The protection of the cell wall was deteriorated by an oxidative damage of the underlying cytoplasmic membrane. The reaction progressively increased the cell permeability, subsequently allowed the free efflux of intracellular contents and eventually led to the cell death [4,13].

TEM image (Fig. 5) confirmed that some TiO<sub>2</sub> NPs migrated through the cell wall to inside the bacterial cells which caused the subsequent direct attack of intracellular components and accelerated the cell death [3,4]. Even in the dark condition, bacterial growth inhibition was also observed due to the additional mechanism. The corresponding results have been reported by mammalian cytotoxicity studies, where TiO<sub>2</sub> exerted oxidative stress in the dark under non-photocatalytic conditions [17-19].

### 4. Conclusion

Colloidal TiO<sub>2</sub> NPs were successfully prepared by the sparking process and investigated for their antibacterial properties against *E.coli*. The results show that the obtained NPs have an excellent antibacterial ability under UV light whereas the NPs probably migrated through the cells in the dark which can also lead to the cell death at the longer reaction time.

### Acknowledgements

This work supported by the Thailand Research Fund and the Commission on Higher Education. W. Thongsuwan is grateful for his PhD scholarship from the Commission on Higher Education.

### References

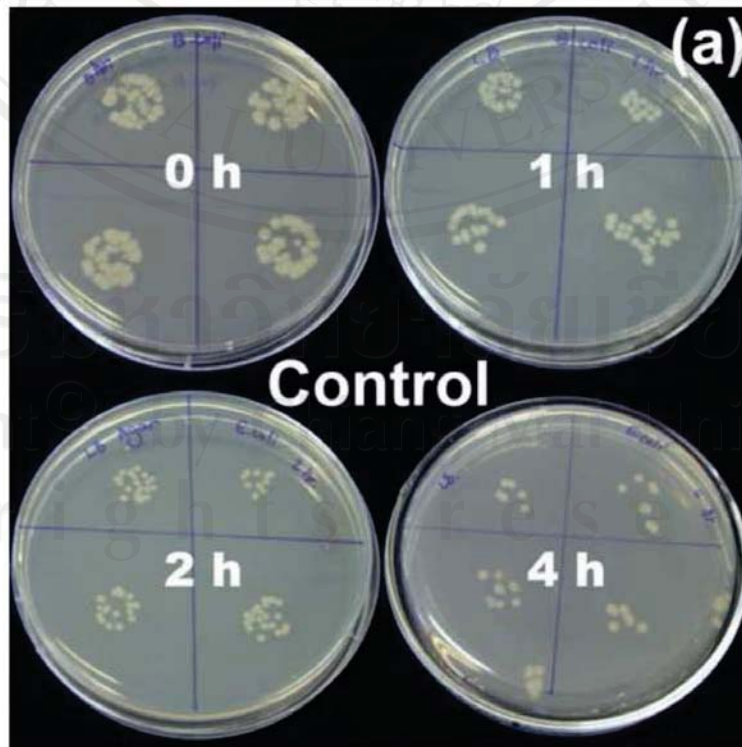
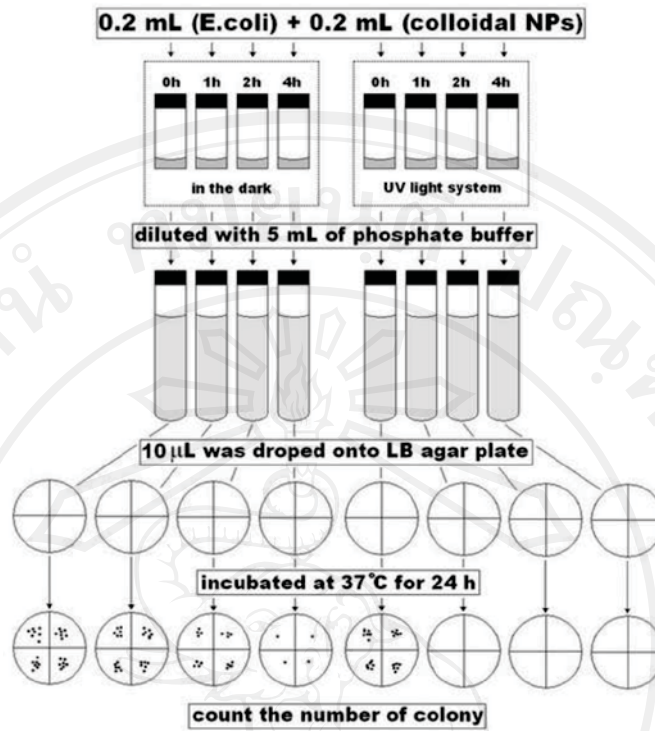
1. C. Guillard, T-H. Bui, C. Felix, V. Moules, B. Lina, P. Lejeune, C.R. Chim. 11 (2008) 107.
2. A. Paleologou, H. Marakas, N.P. Xekoukoulotakis, A. Moya, Y. Vergara, N. Kalogerakis, P. Gikas, D. Mantzavinos, Catal. Today. 129 (2007) 136.
3. Z. Huang, P-C. Maness, D.M. Blake, E.J. Wolfrum, S.L. Smolinski, W.A. Jacoby, J. Photoch. Photobio. A. 130 (2000) 163.
4. H.M. Coleman, C.P. Marquis, J.A. Scott, S.-S. Chin, R. Amal, Chem. Eng. J. 113 (2005) 55.
5. A.K. Benabbou, Z. Derriche, C. Felix, P. Lejeune, C. Guillard, Appl. Catal. B-Environ. 76 (2007) 257.
6. Y. Bessekhouad, D. Robert, J. V. Weber, J. Photoch. Photobio. A. 157 (2003) 47.
7. H. Yang, K. Zhang, R. Shi, X. Li, X. Dong, Y. Yu, J. Alloy. Compd. 413 (2006) 302.
8. K. K. Akurati, A. Vital, G. Fortunato, R. Hany, F. Nueesch, T. Graule, Solid. State. Sci. 9 (2007) 247.
9. B. Gao, Y. Ma, Y. Cao, J. Zhao, J. Yao, J. Solid State Chem. 179 (2006) 41.
10. W. Thongsuwan, T. Kumpika, P. Singjai, Curr. Appl. Phys. 8 (2008) 563.
11. C.C. Trapalis, P. Keivanidis, G. Kordas, M. Zaharescu, M. Crisan, A. Szatvanyi, M. Gartner, Thin Solid Films 433 (2003) 186.
12. H.J. Zhang, D.Z. Wen, Surf. Coat. Tech. 201 (2007) 5720.
13. V.A. Nadtochenko, A.G. Rincon, S.E. Stanca, J. Kiwi, J. Photoch. Photobio. A. 169 (2005) 131.
14. K-J. Shieh, M. Li, Y-H. Lee, S-D. Sheu, Y-T. Liu, Y-C. Wang, Nanomedicine 2 (2006) 121.
15. P.A. Christensen, T.P. Curtis, T.A. Egerton, S.A.M. Kosa, J.R. Tinlin, Appl. Catal. B-Environ. 41 (2003) 371.
16. A.G. Rincon, C. Pulgarin, Appl. Catal. B-Environ. 44 (2003) 263.
17. J-R. Gurr, A.S.S Wang, C-H. Chen, K-Y. Jan, Toxicol. 213 (2005) 66.

18. L.K. Adams, D.Y. Lyon, P.J.J. Alvarez, *Water. Res.* 40 (2006) 3527.  
19. C. Ogino, M.F. Dadjour, K. Takaki, N. Shimizu, *Biochem. Eng. J.* 32 (2006) 100.

### Figure captions

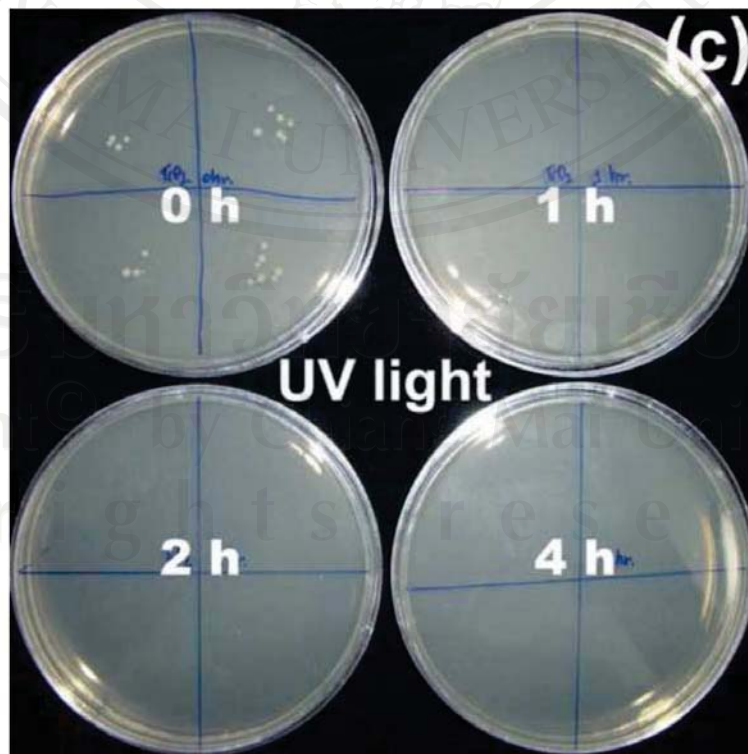
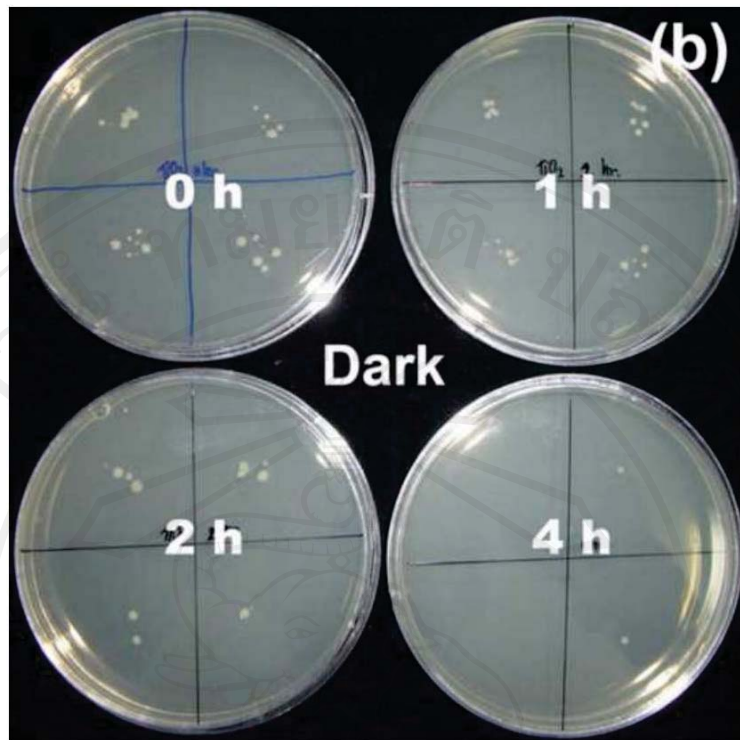
- Fig. 1** Flow chart of the experimental procedures for study of antibacterial activity of TiO<sub>2</sub> NPs.
- Fig. 2** Petri dishes of *E.coli* (a) in UV light without TiO<sub>2</sub> NPs and supplemented with TiO<sub>2</sub> NPs (b) in the dark and (c) under UV light, incubated at reaction times of 0, 1, 2 and 4 h,
- Fig. 3** Plot of the survival rates of *E.coli* against the reaction time in UV light without NPs, supplement with NPs in the dark and under UV light.
- Fig. 4** SEM images of (a) controlled and (b) treated *E.coli* cells with TiO<sub>2</sub> NPs under UV light for 4 h.
- Fig. 5** Cross section TEM image of treated *E.coli* cell with TiO<sub>2</sub> NPs under UV light for 4 h.

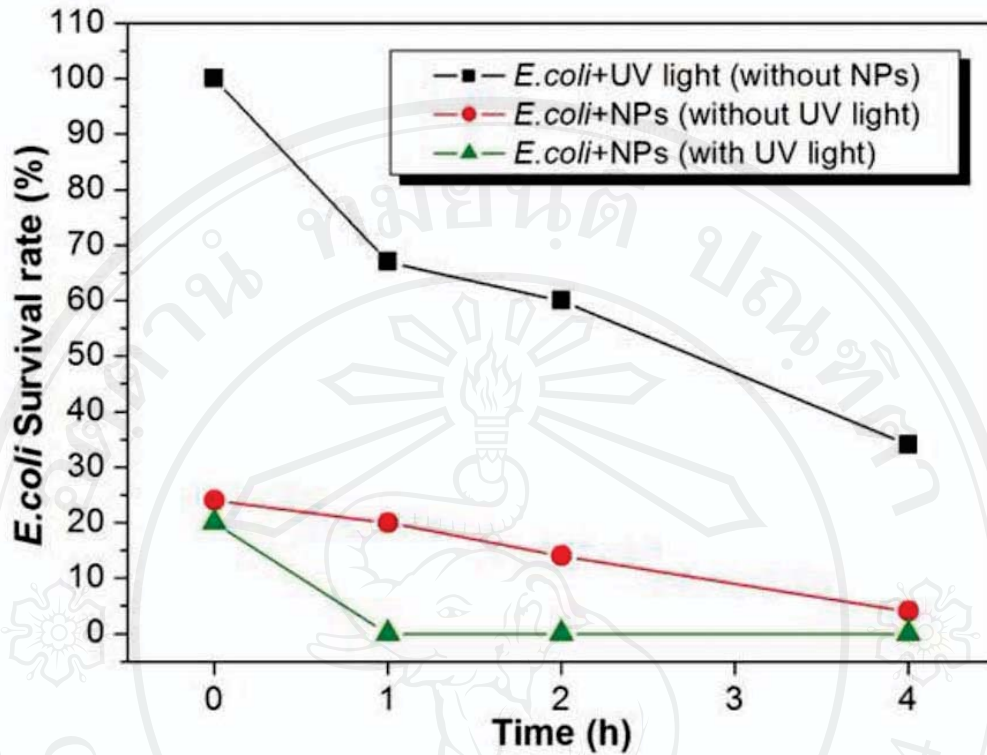




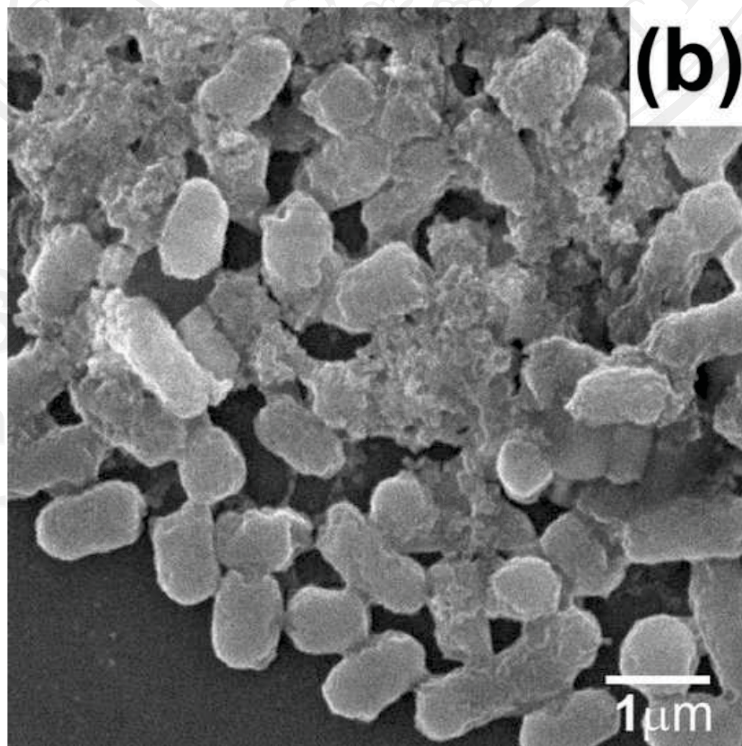
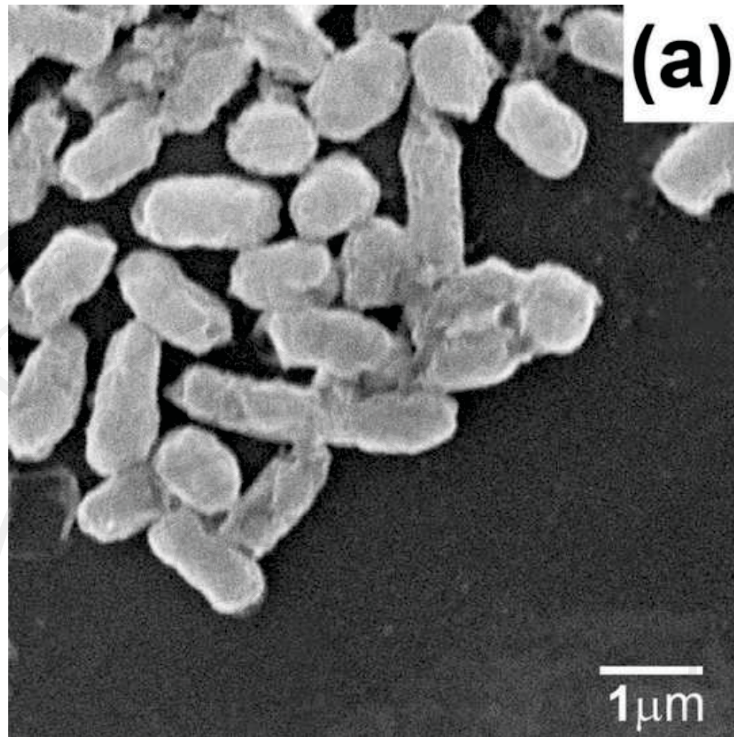
ลิขสิทธิ์  
Copyright  
All rights reserved

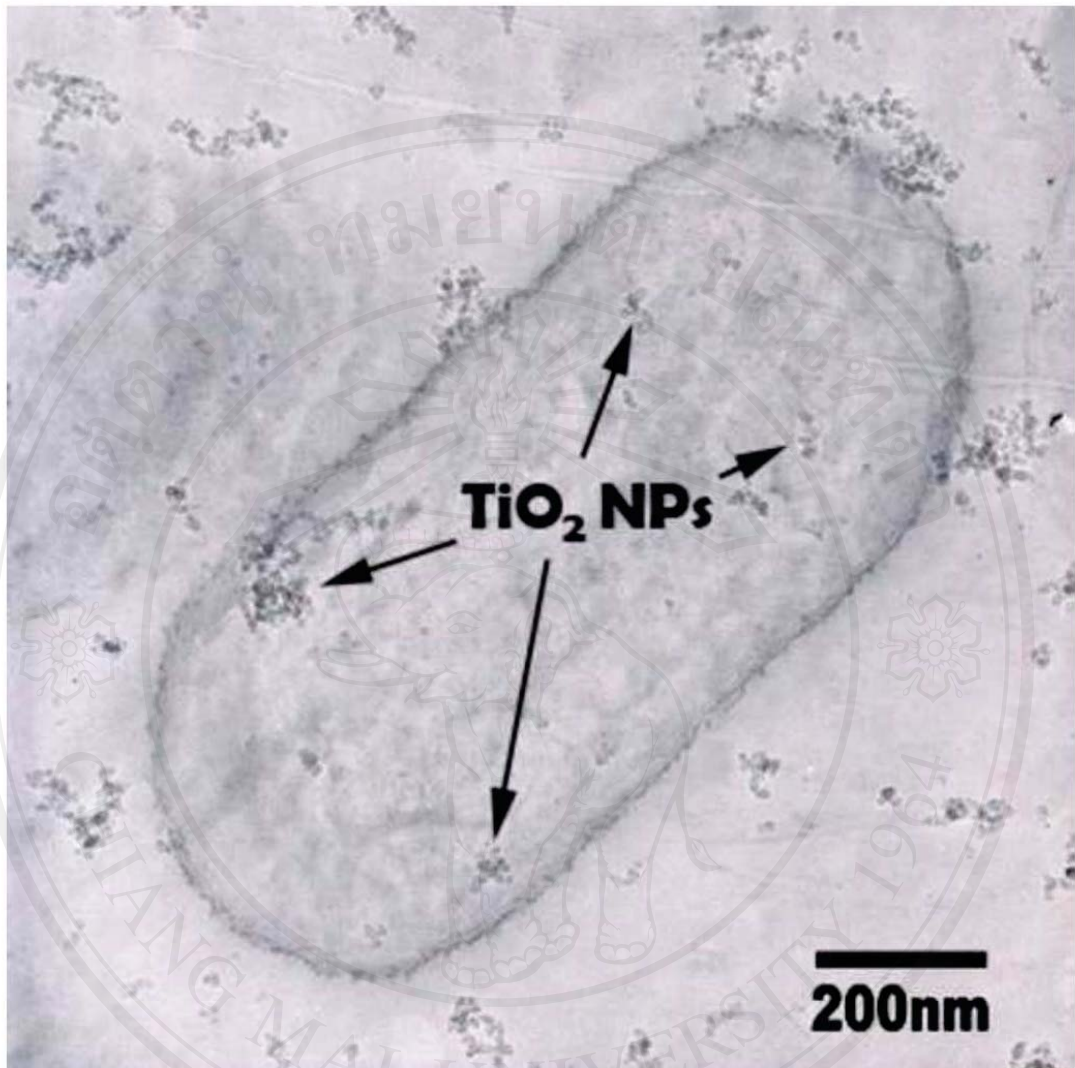
เชียงใหม่  
University  
reserved





ลิขสิทธิ์มหาวิทยาลัยเชียงใหม่  
Copyright© by Chiang Mai University  
All rights reserved





ลิขสิทธิ์มหาวิทยาลัยเชียงใหม่  
Copyright© by Chiang Mai University  
All rights reserved

## Preparation of Iron Oxide Nanoparticles by a Pyrosol Technique

W. Thongsuwan<sup>1, a</sup>, S. Aukkaravittayapun<sup>2, b</sup> and P. Singjai<sup>1, c</sup>

<sup>1</sup>Nanomaterials Research Unit, Department of Physics, Faculty of Science,  
Chiang Mai University, Chiang Mai 50200, Thailand

<sup>2</sup>National Metal and Materials Technology Center, 114 Thailand Science Park,  
Paholyothin Rd. Klong 1, Klong Luang, Pathumthani 12120, Thailand

<sup>a</sup>weeradate@yahoo.com, <sup>b</sup>suparek@mtec.or.th, <sup>c</sup>singjai@cmu.ac.th

**Keywords:** Iron oxide; nanoparticles; pyrosol.

**Abstract.** Iron oxide nanoparticles were prepared from an iron nitrate solution by a pyrosol technique. The precursor solution was atomized by a mist generator in order to form an aerosol which was brought into a tube furnace by a controlled flowing air stream. The pyrolysis of the aerosol was occurred to form the particles inside the furnace at 350 °C. Scanning electron microscopy images have shown that a mean diameter of the particles is in good agreement with the third root of the precursor concentration. X-ray diffraction patterns have revealed that the main peaks from the samples are corresponding to the  $\alpha$ -Fe<sub>2</sub>O<sub>3</sub> phase.

### Introduction

During the last two decades, nanoparticles have received increasing attention due to their unique properties [1, 2]. Iron oxide nanoparticles are well known starting materials which are used as catalysts for carbon nanotube synthesis [3, 4]. Although, the catalysts are commercially available, but they are expensive which may not bring the price of carbon nanotubes down. Several groups have reported methods for synthesis of metal oxide nanoparticles such as a citrate pyrolysis method [5], a low-temperature hydrothermal method [6, 7], a flow injection synthesis technique [8], a chemical vapor deposition method [9], a sol-gel process [10], a pulsed laser evaporation method [11], a sputtering technique [12] and a spray pyrolysis method [13-16].

To our knowledge, there are some reports using a pyrosol method for this purpose [17, 18]. In this work, we have developed an alternative configuration of the pyrosol method which is a very simple and low-cost scheme to produce iron oxide nanoparticles. The products, prepared from various concentrations of iron nitrate were characterized by scanning electron microscopy (SEM) and X-ray diffraction (XRD).

### Experimental

The experiment was carried out using a tube furnace, sized of 19 mm in internal diameter and 750 mm in length (Fig. 1). The tube was connected to a three way tube containing an aqueous iron (III) nitrate (Fe(NO<sub>3</sub>)<sub>3</sub>·9H<sub>2</sub>O) solution at concentrations of 1, 0.1 and 0.01 M. A mist generator (1.7 MHz) was immersed in water and placed under the solution, which was separated from water using a plastic film. The solution was then atomized by the mist generator. The aerosol was subsequently brought into the tube furnace by a controlled flowing air stream (340 ml/min) at 350 °C. The products, formed inside the tube were collected and characterized by SEM (JEOL, JSM-6335F) and XRD (Bruker D8Advance) using Cu-K $\alpha$  radiation operated at 40 kV, 30 mA.

### Results and discussion

An individual spherical particle is apparently seen in the SEM images as shown in Fig. 2a, 1b and 1c for the samples prepared from the precursor concentrations of 1, 0.1 and 0.01 M, respectively. The corresponding size distributions were also given in Fig. 2d, 1e and 1f with mean diameters of approximately 850, 380 and 180 nm, respectively. The mean diameter decreased approximately two

times with decreasing the precursor solution ten times (Fig. 3). It is noted that, the experimental result is in good agreement with the theoretical relation in which the particle size ( $D$ ) is related to the third root of the precursor concentration ( $C$ ) [19, 20].

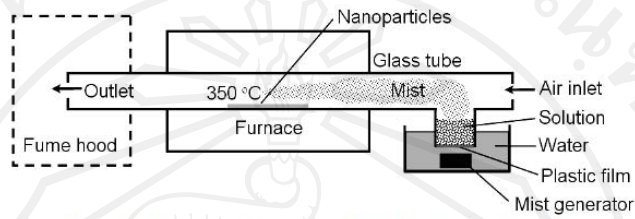


Fig. 1 Schematic diagram of the pyrosol apparatus

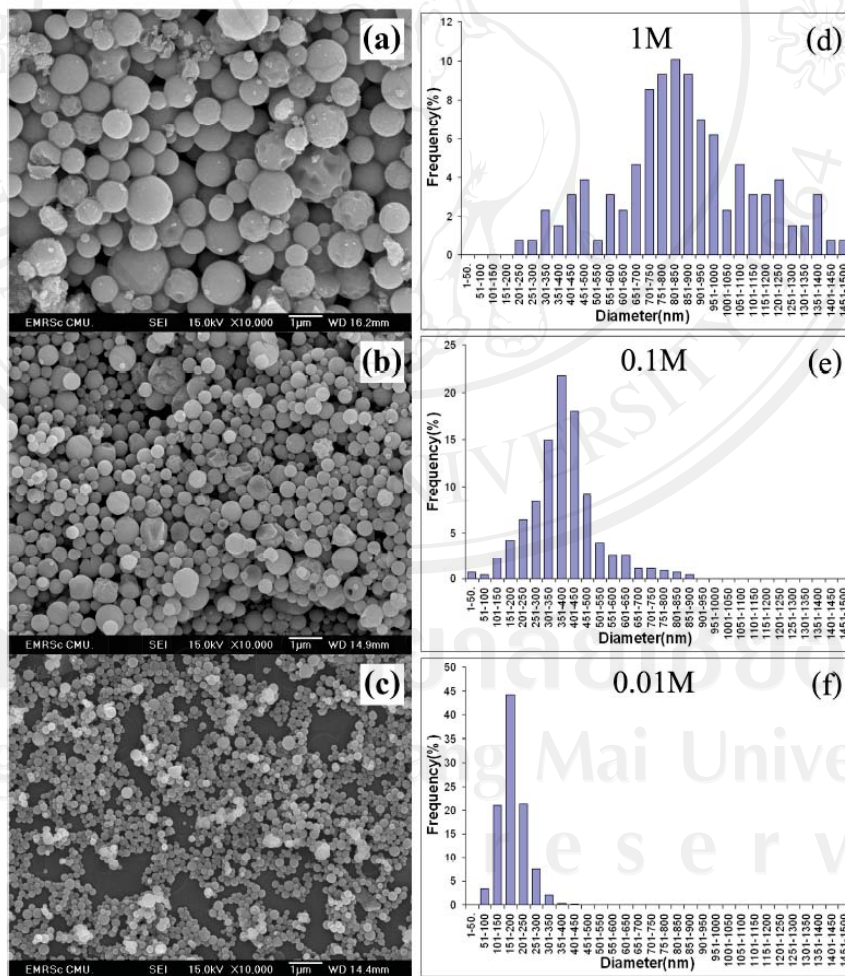


Fig. 2 SEM images of the samples prepared from precursor concentrations of (a) 1, (b) 0.1 and (c) 0.01 M and the corresponding size distributions of (d) 1, (e) 0.1 and (f) 0.01 M, respectively

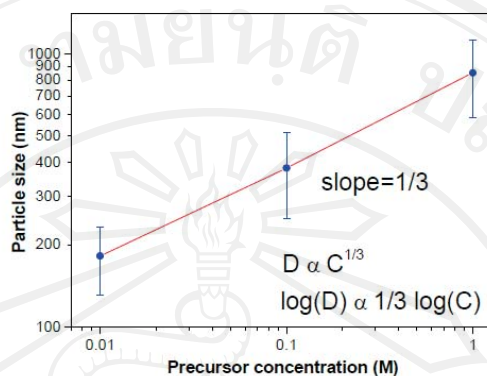


Fig. 3 A linear relation of the experimental mean diameters and the precursor concentrations on logarithmic scales

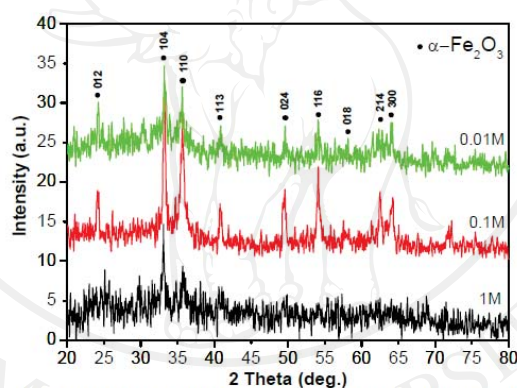


Fig. 4 XRD patterns of  $\alpha$ - $\text{Fe}_2\text{O}_3$  nanoparticles, prepared from various concentration conditions

The XRD patterns (Fig. 4) have revealed that the peaks are corresponding to the  $\alpha$ - $\text{Fe}_2\text{O}_3$  phase (Hematite, JCPDF file 89-0599), with lattice parameters  $a=0.5032$  and  $c=1.3733$  nm. It is noted that the peak heights from the sample prepared with the 1M condition are low. The poor crystallinity is probably originated by the large particle size. On the other hand, the samples obtained from the 0.1 and 0.01M conditions are better crystallized.

### Conclusions

Iron oxide nanoparticles were successfully synthesized from the aqueous iron nitrate solution by the simple and low cost pyrosol technique. The experimental result is in good agreement with the theoretical relation in which the particle size is related to the third root of the precursor concentration. The XRD peaks from the as-prepared samples are corresponding to the  $\alpha$ - $\text{Fe}_2\text{O}_3$  phase.

### Acknowledgments

This work was supported by the Thailand Research Fund and the Commission on Higher Education. The authors would like to thank Ms. Boontarika Srithai for her helps in XRD measurement. W.T. is grateful for his PhD scholarship from the Commission on Higher Education of Thailand under the staff development project.



**References**

- [1] T. Takagahara, E. Hanamura, *Phys. Rev. Lett.* 56 (1986) 2553
- [2] C. Flytzanis, *J. Opt. Soc. Am.* B4 (1987) 6
- [3] S. Honda, Y.G. Baek, K.Y. Lee, T. Ikuno, T. Kuzuoka, J.T. Ryu, S. Ohkura, M. Katayama, K. Aoki, T. Hirao, K. Oura, *Thin Solid Films* 464-465 (2004) 290
- [4] N. S. Kim, Y. T. Lee, J. Park, H. Ryu, H. J. Lee, S. Y. Choi, J. Choo, *J. Phys. Chem.* 106 (2002) 9286
- [5] X.L. Xu, J.D. Guo, Y.Z. Wang, *Mater. Sci. Eng. B* 77 (2000) 207
- [6] X. Wang, L. Gao, H. Zheng, M. Ji, T. Shen, Z. Zhang, *J. Cryst. Growth* 269 (2004) 489
- [7] Q.W. Chen, Y.T. Qian, *Mater. Res. Bull.* 30 (1995) 443
- [8] G. Salazar-Alvarez, M. Muhammed, A.A. Zagorodni, *Chem. Eng. Sci.* 61 (2006) 4625
- [9] C.C. Chai, J. Peng, B.P. Yan, *Sens. Actuat. B* 34 (1996) 412
- [10] X.Q. Liu, S.W. Tao, Y.S. Shen, *Sens. Actuat. B* 40 (1997) 161
- [11] S. Joshi, R. Nawathey, V.N. Koinkar, *J. Appl. Phys.* 64 (1988) 5647
- [12] J.K. Lin, J.M. Sivertsen, *IEEE T. Magn.* 22 (1986) 50
- [13] A. Lopez, F.J. Lazaro, T. Gonzalez-Carreño, M.P. Morales, C.J. Serna, *J. Magn. Mater.* 140-144 (1995) 383
- [14] Y.T. Qian, C.M. Niu, C. Hannigan, S. Yang, *J. Solid State Chem.* 92 (1991) 208
- [15] Y. Xie, W. Wang, Y.T. Qian, *J. Cryst. Growth* 167 (1996) 656
- [16] K. Nomura, Y. Ujihira, *Thin Solid Films* 128 (1985) 225
- [17] S. Wang, W. Wang, W. Wang, Z. Jiao, J. Liu, Y. Qian, *Sens. Actuat. B* 69 (2000) 22
- [18] Y.H. Choa, J.K. Yang, W.J. Yang, K.H. Auh, *J. Magn. Mater.* 266 (2003) 20
- [19] R.J. Lang, *J. Acoust. Soc. Am.* 43 (1962) 6
- [20] J.M. Nedeljkovic, Z.V. Saponjic, Z. Rakocevic, V. Jakanovic, D.P. Uskokovic, *Nanostruct. Mater.* 9 (1997) 125

## Atomic force microscopy imaging of ZnO nanodots deposited on quartz by sparking off different tip shapes

T. Kumpika, W. Thongsuwan and P. Singjai\*

Nanomaterials Research Unit, Department of Physics, Faculty of Science, Chiang Mai University, Chiang Mai 50200, Thailand

Received 17 May 2006; Revised 28 August 2006; Accepted 30 August 2006

We have demonstrated a simple method for depositing ZnO nanodots on quartz substrates by sparking off different tip shapes at voltages of 2, 4 and 6 kV in air at atmospheric pressure. A comparison was made among the three tip shapes: the sharp tip, the conical tip and the dull tip. The surface morphology was then observed by atomic force microscopy. The mean height of the randomly distributed dots of approximately 8 nm was successfully deposited from the sharp tip at 6 kV. Characterizations by UV–vis spectroscopy and Raman spectroscopy have confirmed the presence of ZnO and the quality improvement by annealing treatments. Moreover, a nucleation mechanism of the nanodot formation is discussed. Copyright © 2006 John Wiley & Sons, Ltd.

**KEYWORDS:** AFM; zinc oxide; nanodots; sparking

### INTRODUCTION

ZnO is an interesting semiconductor for optoelectronic devices and sensors owing to its properties of wide band gap (3.37 eV), high excitonic binding energy (60 meV) and high chemical stability.<sup>1,2</sup> It can be used in a variety of applications, such as gas sensors, solar cells, photodetectors and photodiodes.<sup>3–8</sup> Thus, a variety of ZnO nanostructures have been synthesized by many methods, such as reactive electron beam evaporation,<sup>9–11</sup> metalorganic chemical vapor deposition (MOCVD), ion implantation and the wet-chemical method.<sup>12,13</sup> In particular, the ZnO nanodots (NDs) are normally fabricated through advanced and expensive technologies, such as molecular-beam epitaxy (MBE) and pulsed laser deposition (PLD).<sup>14,15</sup>

We have extensively investigated the simple and low-cost technique, as recently reported by our group, for fabricating iron/iron oxide NDs on glass slides and stainless steel substrates.<sup>16,17</sup> In this present paper, ZnO NDs were deposited on quartz substrates by sparking at various voltages from different tip shapes prepared from a zinc wire. The relationship between the applied voltages and the dot sizes was investigated by atomic force microscopy (AFM). The optical properties and chemical states of the as-deposited NDs and the annealed samples were characterized by UV–vis spectroscopy and Raman spectroscopy.

### EXPERIMENTAL

Before the NDs were formed on quartz substrates (12.7 × 12.7 × 1.0 mm<sup>3</sup>, Ted Pella, Inc., Redding, CA) by the high-voltage discharge (sparking) through the zinc tip, the

substrates were sonically cleaned in acetone, distilled water and ethanol, and dried by blowing nitrogen gas. Different tip shapes were prepared from the zinc wire (Ø 0.38 mm, purity 99.97%, Advent Research Material Ltd) by three methods: (i) electrochemical etching for the conical tip; in brief the zinc wire was partially dipped into a 2.5 M KOH solution and was anodically dissolved at 6 volts, (ii) cutting with pliers for a sharp tip and (iii) polishing with an abrasive paper for the dull tip, as photographically depicted in Fig. 1. The prepared tip was then placed vertically at ~3 mm above another zinc wire which was placed horizontally on the quartz substrate (Fig. 2). After a 0.1 µF capacitor was charged to the desired voltages (2, 4 and 6 kV), the tip was gradually moved downward to the substrate until sparking occurred in ambient air at atmospheric pressure.

Surface characterization was done by using an AFM in the tapping mode (Digital Instruments, Inc., Santa Barbara, CA) equipped with a standard Si tip and operated at a scan size of 1 × 1 µm<sup>2</sup> in air at room temperature. Section analysis was carried out to estimate sizes of the NDs using the Nanoscope IIIa 5.12r3 software. The thin film thickness of the NDs was determined from the cross-section scanning electron microscope (SEM) images of the samples prepared by the sparking for over 100 times. The energy gap and chemical state of the as-deposited NDs before and after annealing treatments at 310, 380 and 450 °C for 1 h were investigated by UV–vis spectroscopy (Jasco V-530) over a spectral range from 200 to 1100 nm and by Raman spectroscopy (Horiba Jobin Yvon T64000) with a 514 nm argon ion laser at room temperature.

### RESULTS AND DISCUSSION

#### Effect of electrode polarity

Optical microscope images of the conical tip after the sparking occurred are shown in Fig. 3, where the conical

\*Correspondence to: P. Singjai, Nanomaterials Research Unit, Department of Physics, Faculty of Science, Chiang Mai University, Chiang Mai 50200, Thailand. E-mail: singjai@chiangmai.ac.th

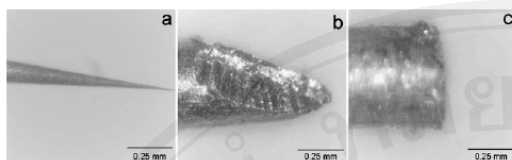


Figure 1. Optical microscope images of (a) the conical tip, (b) the sharp tip and (c) the dull tip.

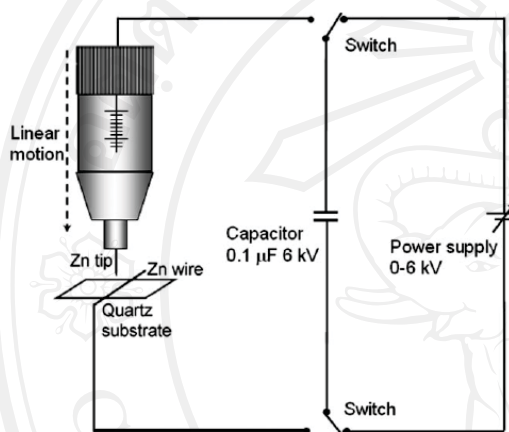


Figure 2. Schematic diagram of the sparking apparatus.

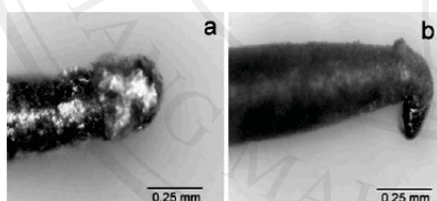


Figure 3. Optical microscope images of (a) the anode tip and (b) the cathode tip after the sparking occurred.

tip was connected to the capacitor (a) as the anode and (b) as the cathode. While achieving a higher deposition rate, it should be noted that an erosion of the anode tip was clearly seen, whereas the cathode tip was bent and slightly eroded. On the basis of this result, the anodic tip was selected for depositing ZnO NDs on the quartz substrates.

#### Surface morphology as imaged by AFM

The deposited NDs cover a macroscopic area of approximately  $7 \text{ mm}^2$  (diameter of  $\sim 3 \text{ mm}$ ) and a few co-deposited microdots were observed by an optical microscope. A comparison of AFM images is shown in Fig. 4(a), (b) and (c), in which the NDs were prepared by sparking once at 4 kV from the conical tip, the sharp tip and the dull tip, respectively. It is noted that the NDs prepared from the dull tip have the largest mean sizes, whereas those prepared from the sharp tip and the conical tip have slightly different mean sizes. From a more detailed information from section analysis of Fig. 4, the mean sizes of ZnO NDs prepared from the conical,

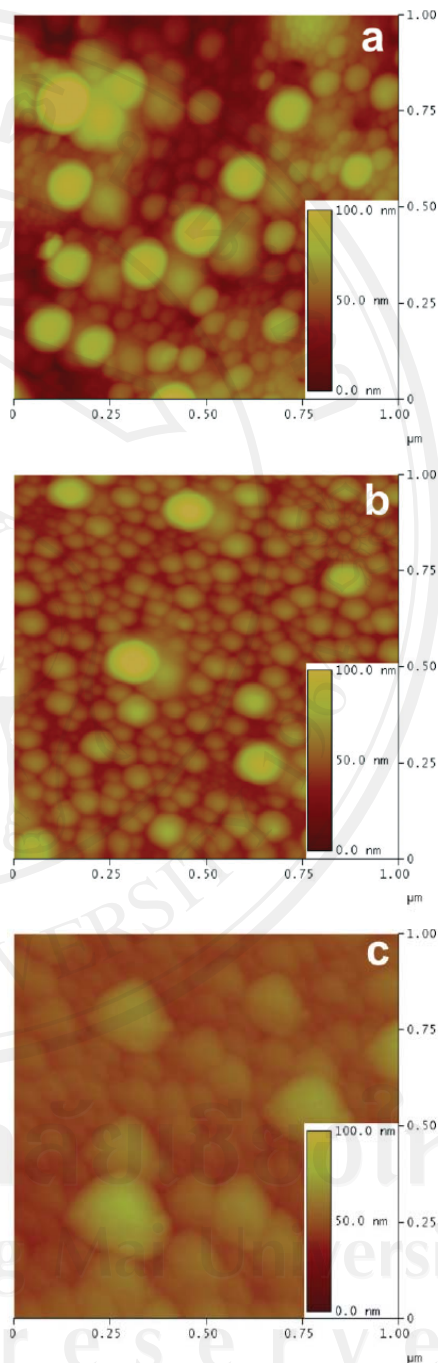
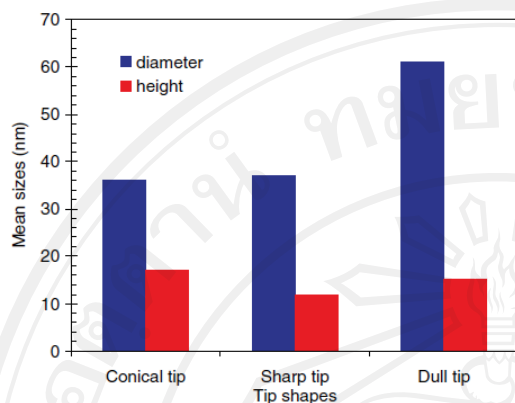


Figure 4. AFM images of ZnO NDs prepared by sparking once at 4 kV from (a) the conical tip (b) the sharp tip and (c) the dull tip.

the sharp and the dull tips were approximately 36, 37 and 61 nm in diameter and 17, 12, 15 nm in height, respectively

T. Kumpika, W. Thongsuwan and P. Singjai



**Figure 5.** The mean heights and the mean diameters of ZnO NDs prepared by sparking once from the different tip shapes at 4 kV, estimated by the section analysis of Fig. 4.

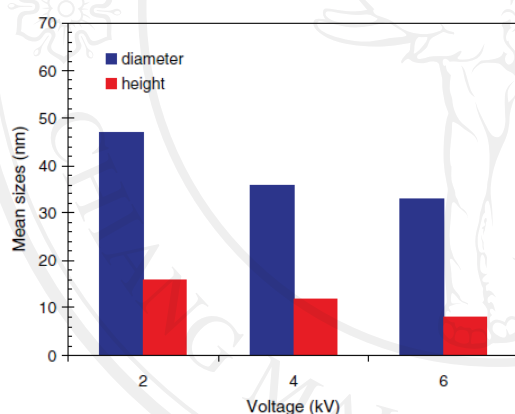


**Figure 6.** The mean heights and the mean diameters of ZnO NDs prepared by sparking once from the sharp tip at 2, 4 and 6 kV.

(Fig. 5). However, one should bear in mind that the diameter, as the lateral size of the NDs estimated from such an AFM image, has undergone a broadening effect by a tip-shape convolution.<sup>18</sup> Therefore, the real diameters are lower than the above results. In order to achieve the lowest sizes, the sharp tip was considered to be the optimum choice and will be used for further investigations.

As suggested above, the sharp tip was selected to study the relationship between the strength of applied voltages and the mean sizes of the NDs. The result is shown in Fig. 6; the mean diameters and the mean heights prepared at 2, 4 and 6 kV were approximately 41, 36 and 34 nm and 16, 12 and 8 nm, respectively. It is clearly seen that sparking at a voltage of 6 kV has deposited the lowest mean sizes and moderate size distributions, as shown in Fig. 7. We understand that, from a thermodynamic point of view, a high specific surface energy is governed by the associated energy stored in such a system.<sup>19</sup> Since the electric energy stored in a capacitor is

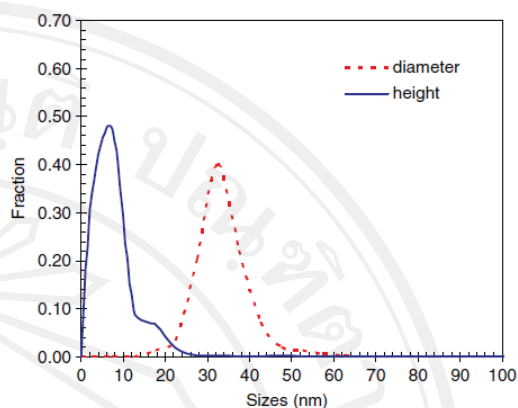


**Figure 7.** Size distributions of ZnO NDs prepared by sparking once from the sharp tip at 6 kV, at which the lowest mean sizes were obtained.

$E = 1/2CV^2$ , by sparking at 6 kV the tip has transferred the highest energy. This supports that the lower mean sizes of the NDs were successfully deposited at the higher voltages.

Under the same deposition conditions, ND thin films were also fabricated by sparking from the sharp zinc tip at 6 kV for over 100 times, at which stacking of the NDs occurred. The film thickness/number of sparks ratio of  $\sim 1.06$  nm/spark was observed by means of the SEM cross-section image (data not shown). Therefore, this present technique can be used to form ND thin films of various metals and metal-oxide semiconductors at any desired thickness depending on requirements of applications and characterizations.

#### UV-vis spectra

The UV-vis spectral range from 200 to 1100 nm was measured from the samples prepared by sparking 30 times, which corresponded to the film thickness of  $\sim 32$  nm. Figures 8 and 9 show the transmittance and the absorbance curves before and after the annealing treatments at 310, 380 and 450 °C. The bandgap can be determined from the plot of  $(\alpha h\nu)^2$  versus the photon energy ( $h\nu$ ) (Fig. 10) from the extrapolation of the linear portion with the energy axis, where  $\alpha$  is the absorption coefficient, as described in Refs 20–22. From the results, the as-deposited and the annealed samples have the bandgaps shown in Table 1. It is noted that the bandgaps determined from the various  $\alpha$ 's were slightly different. The bandgap of the as-deposited sample is as high as 5.60 eV, whereas those of the annealed samples (3.34–3.20 eV) are slightly red-shifted from the classical bandgap of ZnO (3.37 eV).

According to the bandgap observed from our unannealed sample, an explanation was given by Zhou and coworkers<sup>23</sup> concerning ZnO quantum dots prepared from a wet-chemical method. Typically, the as-prepared dots is passivated by an outer thin layer of  $Zn(OH)_2$  in which it increases the energy band gap. We anticipate that the sparking for depositing Zn/ZnO NDs in air at room temperature took place in incomplete oxidation and humidity, i.e. the

**Table 1.** The bandgaps of ZnO samples estimated from different absorption coefficients ( $\alpha$ ):  $t$  is the film thickness (nm),  $R$  is the reflectance,  $T$  is the transmittance,  $C$  is the reflection coefficient ( $C = 10^{-A}$ ) and  $A$  is the absorbance

Samples	Bandgaps (eV)		
	$\alpha_1 = \frac{1}{t} \ln \left( \frac{1-R}{T} \right)$	$\alpha_2 = \frac{(1-C)^2}{2C}$	$\alpha_3 = \ln \frac{1}{T}$
As-deposited	5.62	5.70	5.60
450 °C	3.33	3.34	3.26
380 °C	3.30	3.32	3.23
310 °C	3.26	3.29	3.20

$\alpha_1$  as in Ref. 20.

$\alpha_2$  as in Ref. 21.

$\alpha_3$  as in Ref. 22.

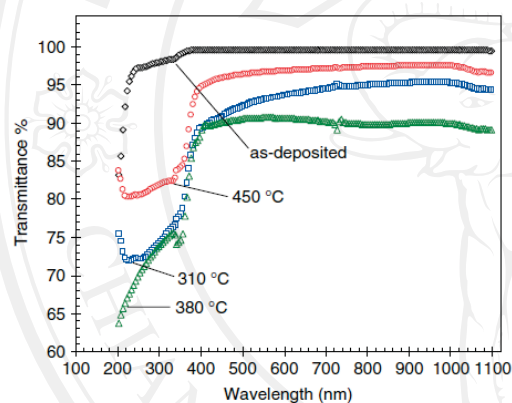


**Figure 8.** Optical transmittance of ZnO NDs prepared by sparking 30 times from the sharp tip at 6 kV and annealing treatments at 310, 380 and 450 °C for 1 h in air.

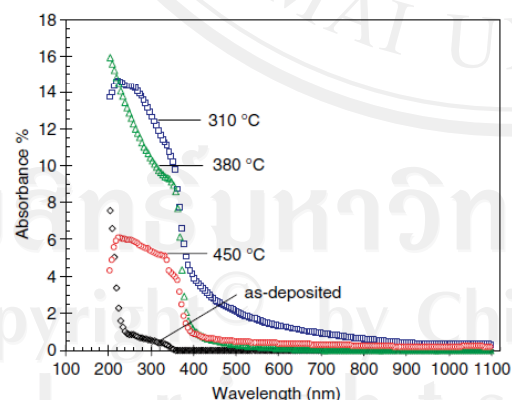


**Figure 9.** Optical absorbance of ZnO NDs: the sample preparation conditions as in Fig. 8.

Zn/ZnO/Zn(OH)<sub>2</sub> core-shell-shell structure was probably formed. Therefore, an annealing treatment is needed for obtaining good quality of the ND thin films prepared by this

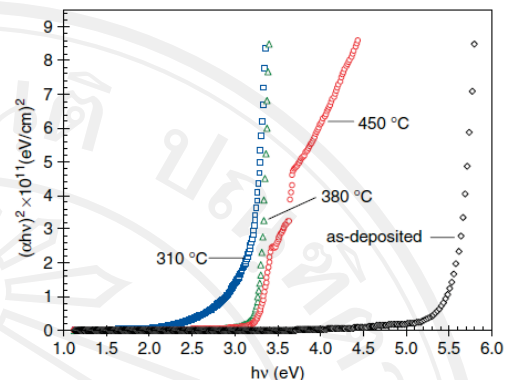


**Figure 10.**  $(ah\nu)^2$  as a function of the photon energy ( $h\nu$ ) for ZnO NDs,  $\alpha$  being the same as in Ref. 20 where the film thickness of 32 nm was estimated from the SEM cross-section image: sample preparation conditions were as in Fig. 8.

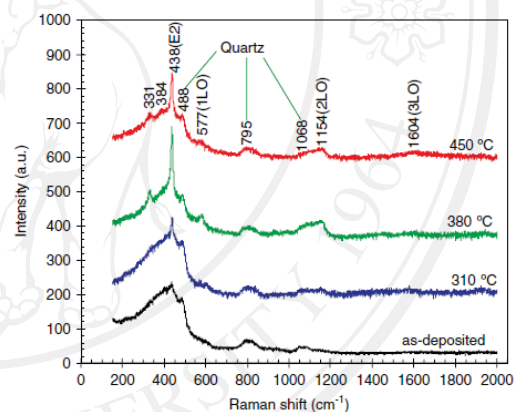


**Figure 11.** Raman spectra of ZnO NDs prepared by sparking 700 times from the sharp tip at 6 kV under the annealing conditions as in Fig. 8.

present method. In addition, the bandgaps of the annealed samples are slightly blue-shifted with increasing annealing temperatures from 310 to 450 °C. In contrast with the previous report,<sup>23</sup> a red-shift from 150 to 500 °C was observed.

#### Raman spectra

Raman scattering was measured from the sample prepared by sparking 700 times, which corresponded to the film thickness of  $\sim 750$  nm. Figure 11 shows the Raman spectra before and after the annealing treatments. The Raman peaks at 438, 577, 1154 and 1604  $\text{cm}^{-1}$  are attributed to the  $E_2$  (high),  $A_1$  longitudinal optical (1LO) phonons, the 2LO phonons and the 3LO phonons of ZnO.<sup>24,25</sup> The small 3LO peak was only observed from the annealing treatment at 450 °C, which indicates that the ND thin films have a partially bulk-like structure.<sup>25</sup> It is noted that the broad plateau from 200 to 600  $\text{cm}^{-1}$  and the peaks at 488 and 795  $\text{cm}^{-1}$  were obtained from the quartz substrate. Therefore, their heights and shapes

T. Kumpika, W. Thongsuwan and P. Singjai

were likely unchanged by the annealing treatments. It should also be pointed that the peaks at 1068 and 1154  $\text{cm}^{-1}$  were obtained from both the ZnO and the quartz substrates. While comparing all spectra of ZnO, the peak heights from the annealed sample at 380 °C are greater than those at the others. Therefore, an optimum annealing temperature for good quality ZnO NDs is suggested.

### Nucleation mechanism

In order to understand a nucleation mechanism of the ND formation, the Zn tip was observed during the sparking under an optical microscope. Interestingly, we found that the Zn tip was melting. The bombardment of high-energy electrons accelerated by a high voltage across the Zn sharp tip and the Zn wire, as shown in Fig. 12, caused high temperature and pressure on molten Zn at the tip surface. Hence, Zn nanodroplets were nucleated, which moved towards the substrate by the high kinetic energy and oxidized in atmospheric air. The particle size of the nanodroplet can be described thermodynamically with the Young–Laplace equation, i.e.  $\Delta P = 2\gamma/r$  where  $r$  is the radius of curvature,  $\gamma$  is surface free energy of the molten Zn and  $\Delta P$  is the pressure difference between inside ( $P_{\text{in}}$ ) and outside ( $P_{\text{out}}$ ) the droplet.<sup>26</sup> Therefore, at a higher applied voltage, the NDs deposited has a smaller mean size. In other words, the mean particle size can be varied by adjusting strength of the applied voltage. Furthermore, the mean particle size can be decreased by increasing the local electric field ( $E_{\text{local}}$ ) at the Zn tip, as the fields at the sharp and conical tips are more enhanced by the field enhancement factor ( $\beta$ ) than at the dull tip.<sup>27</sup>

The above results demonstrate that the Raman spectra of the annealed samples clearly reveal a chemical fingerprint of the ZnO phase. However, our results obtained by this technique may not be used to provide detailed chemical confirmation of the films throughout the thickness. In further work, a depth profile analysis using a surface sensitive technique, such as X-ray photoelectron spectroscopy, will

be carried out for both annealed and unannealed samples. Moreover, the effects of changing the background pressure of dry air or even the effects of different relative humidity conditions on the particle size of the NDs, the chemical states and the quality of the films will be examined.

### CONCLUSIONS

ZnO nanodots were successfully deposited on quartz substrates by the sparking method. The surface morphology as imaged by AFM has shown that sparking from the sharp tip at 6 kV produced the lowest mean height of 8 nm. After the annealing treatments, the Raman spectra showed the optimum annealing temperature to be 380 °C, whereas the UV–vis spectra gave the corresponding bandgap, which showed a slight red-shift from the classical bandgap of ZnO. Thus, we suggest that this simple technique can be utilized to fabricate many other metal/metal-oxide NDs and ND thin films on any arbitrary substrate.

### Acknowledgements

This work was supported by the Thailand Research Fund and the Commission on Higher Education. The authors would like to thank Mr. Ekkapong Kuntarak for his help in Raman spectroscopy measurements. T.K. is grateful for a PhD scholarship from the Commission on Higher Education.

### REFERENCES

- Huang MH, Mao S, Feick H, Yan HQ, Wu YY, Kind H, Weber E, Russo R, Yang PD. *Science* 2001; 292: 1897.
- Chik H, Liang J, Cloutier SG, Kouklin N, Xu JM. *Appl. Phys. Lett.* 2004; 84: 3376.
- Xu H, Liu X, Cui D, Li M, Jiang M. *Sens. Actuators, B* 2006; 114: 301.
- Tang H, Yan M, Ma X, Zhang H, Wang M, Yang D. *Sens. Actuators, B* 2006; 113: 324.
- Cheng XL, Zhao H, Huo LH, Gao S, Zhao JG. *Sens. Actuators, B* 2004; 102: 248.
- Baxter JB, Aydil ES. *Sol. Energy Mater. Sol. Cells* 2006; 90: 607.
- Jeong IS, Kim JH, Park H, Im S. *Thin Solid Films* 2004; 447–448: 111.
- Lee JY, Choi YS, Choi WH, Yeom HW, Yoon YK, Kim JH, Im S. *Thin Solid Films* 2002; 420–421: 112.
- Wu HZ, Qiu DJ, Cai YJ, Xu XL, Chen NB. *J. Cryst. Growth* 2002; 254: 50.
- Xu WL, Zheng MJ, Ding GQ, Shen WZ. *Chem. Phys. Lett.* 2005; 411: 37.
- Giannakopoulos K, Boukos N, Travlos A. *Superlattices Microstruct.* 2006; 39: 115.
- Amekura H, Umeda N, Yoshitake M, Kono K, Kishimoto N, Buchal CH. *J. Cryst. Growth* 2006; 287: 2.
- Dantas NO, Monte AFG, Cardoso WA, Brito-Madurro AG, Madurro JM, Morais PC. *Microelectr. J.* 2005; 36: 234.
- Mei X, Kim D, Ruda HE, Guo QX. *Appl. Phys. Lett.* 2002; 81: 361.
- Nam W, Seo H, Park SC, Bae CH, Nam SH, Park SM, Ha JS. *Jpn. J. Appl. Phys.* 2004; 43: 7793.
- Thongtem S, Singjai P, Thongtem T, Preyachoti S. *Mater. Sci. Eng., A* 2006; 423: 209.
- Thongtem S, Singjai P, Thongtem T, Daothong S. *Mater. Sci. Forum* 2006; 510–511: 470.
- Castle JE, Zhdan PA, Singjai P. *J. Phys. D: Appl. Phys.* 1998; 31: 3437.
- Ragone DV. *Thermodynamics of Materials*. John Wiley and Sons: New York, 1995.
- Aly SA, El Sayed NZ, Kaid MA. *Vacuum* 2001; 61: 1.

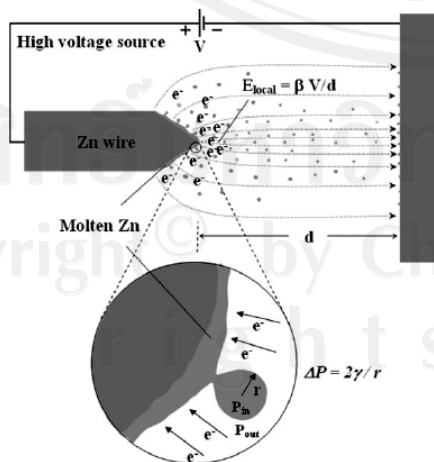
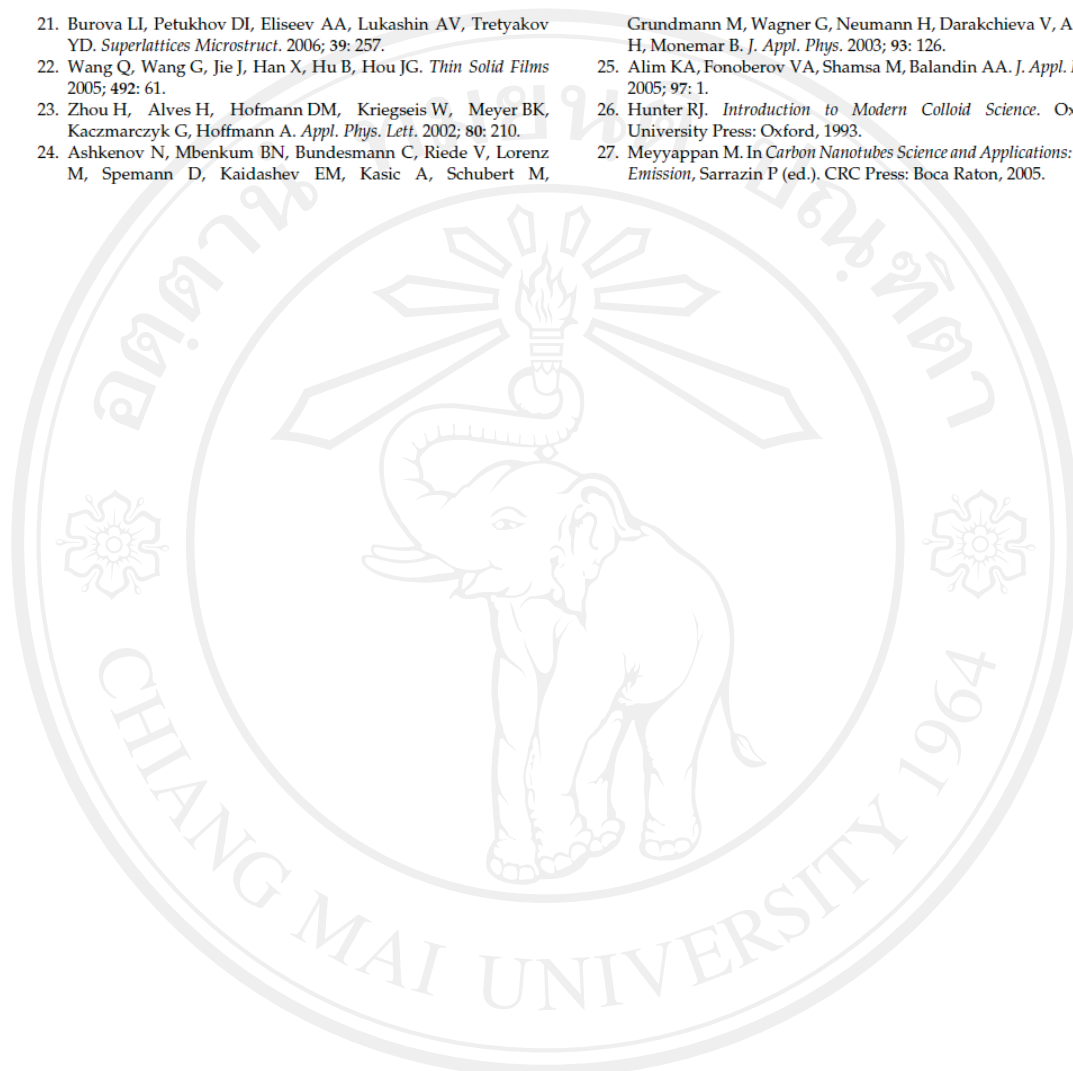


Figure 12. Schematic diagram of the nucleation mechanism of ZnO NDs deposited by the sparking method.

21. Burova LJ, Petukhov DI, Eliseev AA, Lukashin AV, Tretyakov YD. *Superlattices Microstruct.* 2006; 39: 257.
22. Wang Q, Wang G, Jie J, Han X, Hu B, Hou JG. *Thin Solid Films* 2005; 492: 61.
23. Zhou H, Alves H, Hofmann DM, Kriegseis W, Meyer BK, Kaczmarczyk G, Hoffmann A. *Appl. Phys. Lett.* 2002; 80: 210.
24. Ashkenov N, Mbenkum BN, Bundesmann C, Riede V, Lorenz M, Spemann D, Kaidashev EM, Kasic A, Schubert M, Grundmann M, Wagner G, Neumann H, Darakchieva V, Arwin H, Monemar B. *J. Appl. Phys.* 2003; 93: 126.
25. Alim KA, Fonoberov VA, Shamsa M, Balandin AA. *J. Appl. Phys.* 2005; 97: 1.
26. Hunter RJ. *Introduction to Modern Colloid Science.* Oxford University Press: Oxford, 1993.
27. Meyyappan M. In *Carbon Nanotubes Science and Applications: Field Emission*, Sarrazin P (ed.). CRC Press: Boca Raton, 2005.



ลิขสิทธิ์มหาวิทยาลัยเชียงใหม่  
Copyright© by Chiang Mai University  
All rights reserved



## Optical and electrical properties of ZnO nanoparticle thin films deposited on quartz by sparking process

T. Kumpika, W. Thongsuwan, P. Singjai\*

*Nanomaterials Research Unit, Department of Physics, Faculty of Science, Chiang Mai University, Chiang Mai 50200, Thailand*

Available online 13 July 2007

### Abstract

ZnO nanoparticle thin films were deposited on quartz substrates by a novel sparking deposition which is a simple and cost-effective technique. The sparking off two zinc tips above the substrate was done repeatedly 50–200 times through a high voltage of 10 kV in air at atmospheric pressure. The film deposition rate by sparking process was approximately 1.0 nm/spark. The ZnO thin films were characterized by X-ray diffraction, Raman spectroscopy, UV–vis spectrophotometry, and ionoluminescence at room temperature. The two broad emission peaks centered at 483 nm (green emission) and 650 nm (orange-red emission) were varied after two-step annealing treatments at 400–800 °C. Moreover, the electrical resistivity of the films was likely to be proportional to the peak intensity of the orange-red emission.  
© 2007 Elsevier B.V. All rights reserved.

**Keywords:** Zinc oxide; Thin films; Sparking deposition

### 1. Introduction

ZnO is an important II–VI compound semiconductor material due to its direct energy gap and large excitation binding energy at room temperature. It has the unique optical and electrical properties which can be used in a variety of applications, such as high transmittance conductive oxide coatings for solar cells [1], gas sensors [2], UV photodetectors [3], and bulk acoustic wave resonators [4]. To deposit the ZnO films, various methods have been used such as pulsed laser deposition (PLD) [5,6], spray pyrolysis [7,8], and sol–gel process [9]. Among these techniques, spray pyrolysis and sol–gel process are relatively simple and inexpensive methods. In contrast, the high-cost PLD method often gives typically high orientation along *c*-axis as recently reported by Zhao et al. [10].

It is known that low intrinsic defects of single-crystalline ZnO nanostructures are required for applications such as UV-emitting devices [11,12] and UV detectors [13–15]. However, the oxygen vacancy defects, crystal deficiencies and increased specific surface area of ZnO nanostructures have also been extensively investigated owing to their higher active sites for

photocatalytic activities [16–18] and strong green emission characteristic [19–21]. In this work, a novel sparking method to deposit ZnO nanoparticle (NP) thin films on the quartz substrates has been investigated. The structural, optical, and electrical properties of the films were characterized by X-ray diffraction (XRD), ionoluminescence (IL), UV–vis spectrometry, and electrical resistance measurement.

### 2. Experiment

The sparking method for depositing ZnO nanodots was recently reported by our group [22]. However a different scheme using two sharp tips was demonstrated in this present work, as schematically depicted in Fig. 1. The quartz substrates ( $10 \times 10 \times 1$  mm<sup>3</sup>, Ted Pella, Inc., Redding, CA) were sonically cleaned in acetone, distilled water, and ethanol, and then dried by nitrogen gas blowing. The two sharp tips were prepared from the zinc wire ( $\varnothing$  0.38 mm, purity 99.97%, Advent Research Materials Ltd). The tips were then placed horizontally at 3 mm spacing and 2 mm above the center of the substrate. The sparking occurred when the 25 nF capacitor was charged to 10 kV and connected to the two tips by the rotating switch. The experiment was done repeatedly 50–200 times in ambient air at atmospheric pressure with the sparking time of 3 s/spark. From our previous results about nucleation mechanism of nanoparticles by sparking [22],

\* Corresponding author. Tel.: +66 53 941922x610; fax: +66 53 892271.  
E-mail addresses: napnaptace@yahoo.com, singjai@chiangmai.ac.th (P. Singjai).



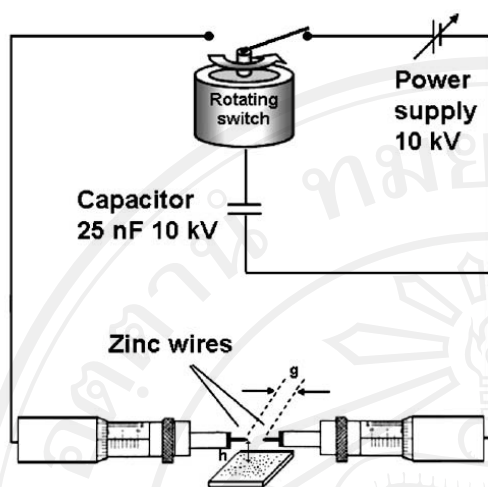


Fig. 1. Schematic diagram of the sparking apparatus.

the as-deposited films were pre-annealed at 380 °C for 1 h and then annealed at 400–800 °C for another 1 h.

The surface morphology, root-mean-square (rms) roughness, and film thickness were characterized by atomic force microscopy (AFM, Digital Instruments, Inc., Santa Barbara, CA) by using tapping mode equipped with a standard Si tip and operate at a scan size of  $1 \times 1 \mu\text{m}^2$  in air at room temperature and scanning electron microscopy (SEM, JEOL JSM 6335F). The crystal structure was investigated by X-ray diffraction (PANalytical X'Pert Pro MPD) using  $\text{CuK}\alpha$  radiation with  $\lambda = 1.54 \text{ \AA}$  operating at 40 kV, 40 mA. The Raman spectra were obtained with a 514.5 nm argon ion laser at room temperature (Jobin Yvon Horiba T64000). The IL spectra were obtained with 1.7 MV  $\text{He}^{2+}$  at room temperature (Tandron accelerator) and Ocean Optic S2000 spectrometer. Optical transmittances were carried out in the range of 300 to 800 nm using UV–vis spectrophotometer (Hitachi U-4100). The electrical resistance of the films was measured between two gold-coated electrodes of 10 mm in length and 2 mm apart at 200 °C.

### 3. Results and discussion

The surface morphology of the as-deposited films, as shown in Fig. 2(a), is rather rough due to the irregular stacking of the particles on the substrate. The corresponding SEM cross-section image, as shown in Fig. 2(b), shows the film thickness of approximately 200 nm after 200 times of sparking. Fig. 2(c) displays the film thickness as a function of the sparking number. It is clearly seen that the film thickness increased linearly from 50 to 200 nm with increasing sparking to 200 times. In other words, the film deposition rate by sparking process was approximately 1.0 nm/spark.

AFM images of the as-deposited and annealed samples (800 °C) were shown in Fig. 3(a) and (b). The rms roughness of 46, 45, 36 and 28 nm and the corresponding grain sizes of 30, 36, 42 and 44 nm were obtained from the as-deposited sample

and the samples annealed at 400, 500 and 800 °C, respectively (Fig. 3c). The grain sizes obtained from AFM images are slightly larger than those observed from SEM images, due to the broadening effect of the tip-shape convolution [23].

XRD patterns as shown in Fig. 4, exhibit polycrystalline structure of hexagonal wurtzite ZnO. Only a broad peak of amorphous quartz was observed from the as-deposited sample. Diffraction peaks ( $2\theta$ ) of the annealed samples at 31.8°, 34.4°, 36.3°, 56.6°, 62.9°, and 67.8° correspond to (100), (002), (101), (110), (103), and (112) planes, respectively. The peak intensities increased with increase in the annealing temperature up to 600 °C at which the ZnO films were well-crystallized. In other words, the transformation of the amorphous phase to the polycrystalline ZnO films mainly occurred at 600 °C. However,

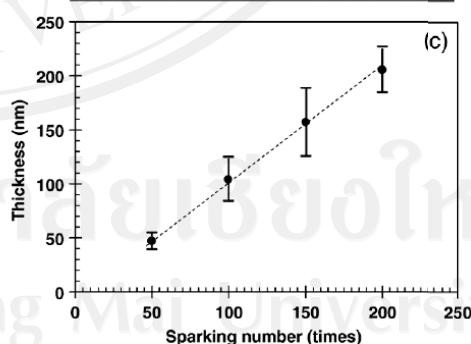
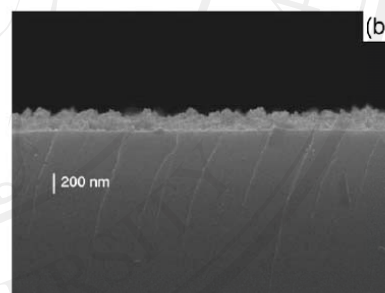
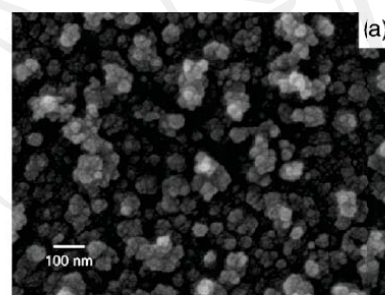


Fig. 2. SEM images of (a) the as-deposited ZnO thin films and (b) the cross section image with sparking number of 200 times. (c) The thickness of the sample as a function of the sparking numbers.

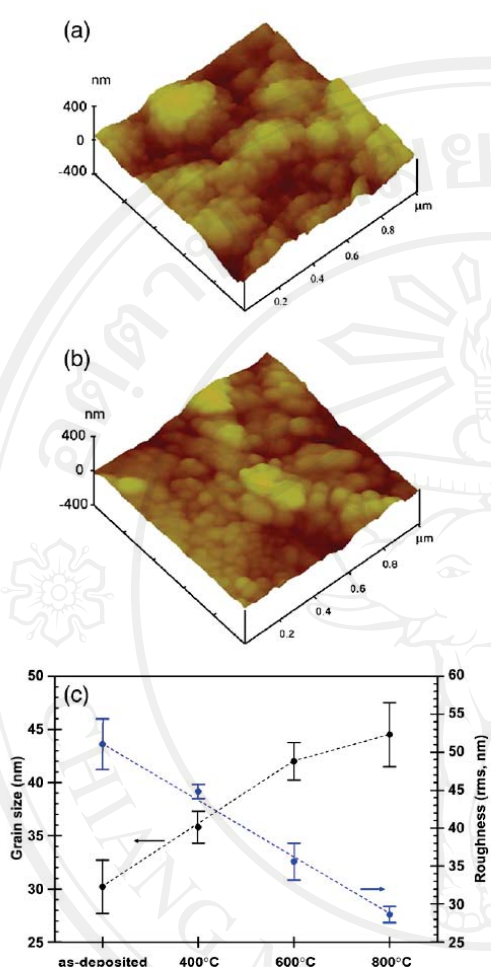


Fig. 3. AFM images of (a) the as-deposited sample and (b) the sample annealed at 800 °C. (c) The grain size and the surface roughness as functions of the annealing temperature.

as the annealing temperature increased further up to 800 °C, the intensities of XRD peaks were decreased. It was ascribed to higher oxygen vacancy defects at that temperature and will be discussed later herein.

Fig. 5 shows Raman spectra of the ZnO films grown by the sparking method with an excitation of 514.5 nm line of argon ion laser. The chemical fingerprint of the ZnO phase was confirmed by the peaks centered at 438, 335, 580, and 1140  $\text{cm}^{-1}$ , which correspond to the  $E_2(\text{high})$ , the second order of Raman scattering, the  $E_1(\text{LO})$ , and the 2LO modes, respectively. It is noted that, the peak intensities corresponding to the ZnO phase increased with increasing the annealing temperature. However, the peaks centered at 490, 800, and 1068  $\text{cm}^{-1}$  are the optical phonon modes of the quartz substrate, of which the peak intensities were likely

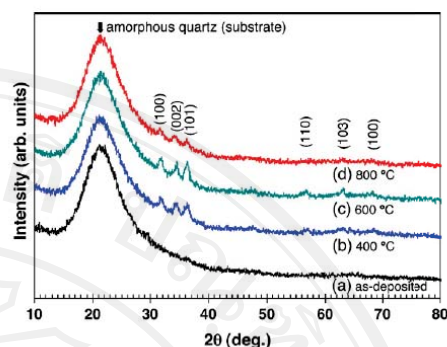


Fig. 4. XRD spectra of ZnO thin films of (a) the as-deposited sample and the samples annealed at (b) 400 °C, (c) 600 °C, and (d) 800 °C.

unchanged by the annealing treatments. IL spectra of ZnO thin films at room temperature consisted of two emission bands as shown in Fig. 6. The green emissions were observed at 483 nm for the as-deposited and the annealed samples at 400 and 600 °C, but 520 nm for the annealed sample at 800 °C. In contrast, the orange-red peaks were observed at 650 nm for all samples. The green band is known as a result of the singly ionized oxygen vacancies [24] whereas the orange-red band corresponds to the excess oxygen atoms (oxygen interstitials) [25]. It is noted that as the annealing temperature increased from 400 to 600 °C, both emission intensities increased. However, for the sample annealed at 800 °C, the green emission peak shifted to a lower energy with increase in its intensity whereas that of the orange-red emission decreased. Because the kinetic energy of atoms in the ZnO lattice was relatively high at high annealing temperature, the escape rate of oxygen atom was greater than the adsorption rate. Consequently, high oxygen vacancies favorably formed in the ZnO lattice. This result was in good agreement with the XRD result in Fig. 4.

Fig. 7 shows the optical transmittance spectra of the films as a function of wavelength. The optical transmittance in the visible region dropped with increasing the annealing temperature to the

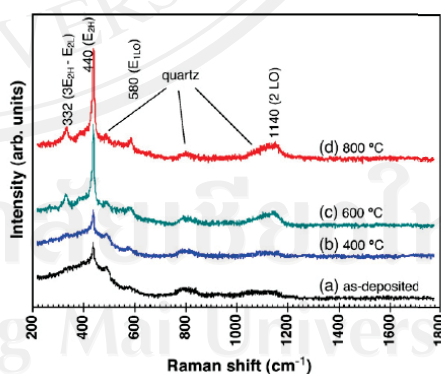


Fig. 5. Raman spectra of ZnO thin films of (a) the as-deposited sample and the samples annealed at (b) 400 °C, (c) 600 °C, and (d) 800 °C.

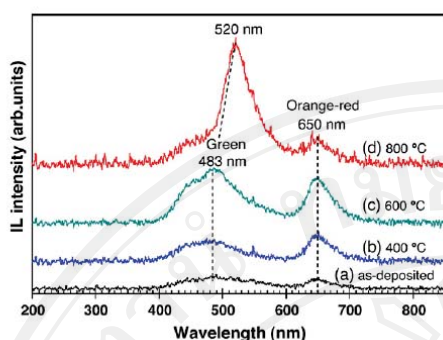


Fig. 6. Ionoluminescence spectra of ZnO thin films of (a) the as-deposited sample and the samples annealed at (b) 400 °C, (c) 600 °C, and (d) 800 °C.

minimum transmittance at 600 °C. Furthermore, the optical transmittance is also related to the film crystallization and orientation, as shown in XRD patterns of Fig. 4 where the increasing of crystallization decreased the optical transmittance. Inset figure shows the plot of  $(\alpha h\nu)^2$  versus  $h\nu$  for obtaining energy gap ( $E_g$ ), where  $\alpha$  is the absorbance coefficient ( $\alpha \sim -\ln T$ ) and  $h\nu$  is the photon energy [26]. The  $E_g$  of 3.43, 3.28, 3.25, and 3.24 eV were estimated for the as-deposited samples and the samples annealed at 400, 600 and 800 °C, respectively. The  $E_g$  of the samples slightly decreased with higher annealing temperature. It was attributed that the formation of  $Zn(OH)_2$  occurred in ambient air, which was subsequently removed by the annealing treatment [26].

Fig. 8 shows the electrical resistivity and the orange-red-emission intensity as a function of the annealing temperature. The resistivity increased from 1.3 to 9.1 k $\Omega$  cm with increasing the annealing temperature from 400 to 600 °C. Since, an ideal defect-free ZnO film is an insulator [27], the well-crystallized sample annealed at 600 °C had high resistivity. However, the annealing treatment at 800 °C decreased the film resistivity as well as the orange-red peak intensity. It is apparently seen that the film

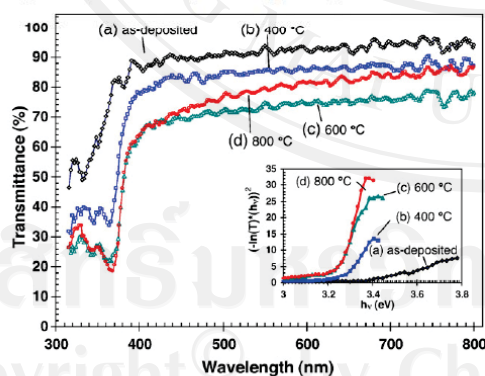


Fig. 7. Optical transmittance spectra of ZnO thin films of (a) the as-deposited sample and the samples annealed at (b) 400 °C, (c) 600 °C, and (d) 800 °C. Inset, the Tauc's plot for estimation of the energy gaps of the films.

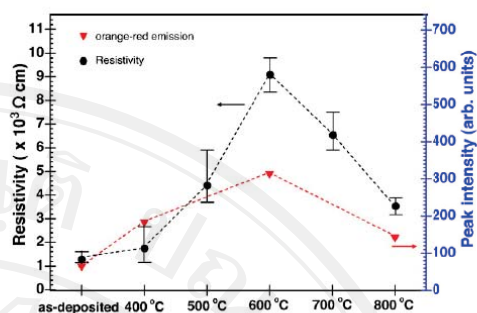


Fig. 8. The electrical resistivity and the intensity of orange-red emission of the ZnO films, as functions of the annealing temperature.

resistivity likely corresponded to the peak intensity of the orange-red emission. It was suggested that the electrical resistivity of ZnO decreased with decreasing the oxygen interstitials.

There is a strong indication of the red-shift of the green emission of ZnO which was previously discussed by many groups [28,29]. Dijken and co-workers [28] reported that it was due to an increasing of the particle size from 0.7 to 1 nm, which led to the decreasing of the  $E_g$ . Moreover, the band filling was recently proposed for the red-shift of green emission with aging time [29]. The later was likely to be the reason for the red-shift in the case of our result. However, further investigation is needed for a better understanding.

We suggest that the sparking of two zinc tips has some advantages over the one tip [22], such as a simplified operation and suitability for a large area substrate by multiple sparking in arrays. In addition, the annealing conditions should be appropriately selected for a desired application. For example, the annealed sample at 800 °C has high potential applications for light emitting devices due to its strong green emission. Whereas the as-deposited and annealed samples at 400 °C have low resistivities and high optical transmittances, therefore, they also have potential applications for electrodes of solar cells and heat mirrors.

#### 4. Conclusions

ZnO thin films were successfully synthesized by the sparking method. The film thickness could be controlled with deposition rate of 1 nm/spark. The rms roughness of the samples decreased with increasing the annealing temperature, whereas the grain size increased. The as-deposited films were mainly amorphous which were transformed to polycrystalline ZnO by the annealing treatments at temperature  $\leq 600$  °C. However, oxygen vacancy defects increased and the red-shift of green emission occurred as the samples were annealed at 800 °C. The magnitude of film resistivity likely corresponded to the peak intensity of the orange-red emission.

#### Acknowledgements

This work was supported by the Thailand Research Fund, the Commission on Higher Education and Graduate School Chiang

Mai University. The authors would like to thank Ion Beam Analysis Laboratory and Mr. Teerasak Kamwanna for their help in ionoluminescence measurement and Mr. Ekkapong Kuntarak for Raman spectroscopy measurement. T. Kumpika is grateful for his PhD scholarship from the Commission on Higher Education.

#### References

- [1] J. Yoo, J. Lee, S. Kim, K. Yoon, I.J. Park, S.K. Dhungel, B. Karunakaran, D. Mangalaraj, J. Yi, *Thin Solid Films* 480–481 (2005) 213.
- [2] H. Xu, X. Liu, D. Cui, M. Li, M. Jiang, *Sens. Actuators, B, Chem.* 114 (2006) 301.
- [3] I.S. Jeong, J.H. Kim, H.-H. Park, S. In, *Thin Solid Films* 447–448 (2004) 111.
- [4] J.P. Atana, R.A. Asmar, A. Khoury, A. Foucaran, *Sens. Actuators, A, Phys.* 127 (2006) 49.
- [5] J.A. Sans, A. Segura, M. Mollar, B. Mari, *Thin Solid Films* 453–454 (2004) 251.
- [6] S. Christoulakis, M. Suchea, M. Katharakis, E. Koudoumas, G. Kiriakidis, *Rev. Adv. Mater. Sci.* 10 (2005) 331.
- [7] A.J.C. Fiddes, K. Durose, A.W. Brinkman, J. Woods, P.D. Coates, A.J. Banister, *J. Cryst. Growth* 159 (1996) 210.
- [8] B.J. Lokhande, P.S. Patil, M.D. Uplane, *Mater. Lett.* 57 (2002) 573.
- [9] Y.Q. Huang, L. Meidong, Z. Yike, L. Churong, X. Donglin, L. Shaobo, *Mater. Sci. Eng., B, Solid-State Mater. Adv. Technol.* 86 (2001) 232.
- [10] J. Zhao, L. Hu, Z. Wang, J. Sun, Z. Wang, *Appl. Surf. Sci.* 253 (2006) 841.
- [11] T. Nagata, P. Ahmet, Y.Z. Yoo, K. Yamada, K. Tsutsui, Y. Wada, T. Chikyow, *Appl. Surf. Sci.* 252 (2006) 2503.
- [12] C. Yuen, S.F. Yu, S.P. Lau, G.C.K. Chen, *J. Cryst. Growth* 287 (2006) 204.
- [13] S. Liang, H. Sheng, Y. Liu, Z. Hao, Y. Lu, H. Shen, *J. Cryst. Growth* 225 (2001) 110.
- [14] C.L. Hsu, S.J. Chang, Y.R. Lin, P.C. Li, T.S. Lin, S.Y. Tsai, T.H. Lu, I.C. Chen, *Chem. Phys. Lett.* 416 (2005) 75.
- [15] T.H. Moon, M.C. Jeong, W. Lee, J.M. Myoung, *Appl. Surf. Sci.* 240 (2005) 280.
- [16] S.B. Park, Y. Kang, *J. Aerosol Sci.* 28 (1997) S473.
- [17] Y. Yamaguchi, M. Yamazaki, S. Yoshihara, T. Shirakashi, *J. Electroanal. Chem.* 442 (1998) 1.
- [18] T. Szabo, J. Nemeth, I. Dekany, *Colloids Surf., A Physicochem. Eng. Asp.* 230 (2004) 23.
- [19] Q.D. Wang, D.H. Zhang, Z.Y. Xue, X.J. Zhang, *Opt. Mater.* 26 (2004) 23.
- [20] Y. Zou, Y. Wang, Z. Chen, J. Wang, Y. Li, *Mater. Lett.* 59 (2005) 3042.
- [21] Z.G. Wang, X.T. Zu, S. Shu, L.M. Wang, *Physica E* 35 (2006) 199.
- [22] T. Kumpika, W. Thongsuwan, P. Singjai, *Surf. Interface Anal.* 39 (2007) 58.
- [23] J.E. Castle, P.A. Zhdan, P. Singjai, *J. Phys. D: Appl. Phys.* 31 (1998) 3437.
- [24] K. Vanheusden, W.L. Warren, C.H. Seager, D.R. Tallant, J.A. Voigt, B.E. Gnade, *J. Appl. Phys.* 79 (1996) 7983.
- [25] E.S. Shim, H.S. Kang, S.S. Pang, J.S. Kang, I. Yun, S.Y. Lee, *Mater. Sci. Eng., B, Solid-State Mater. Adv. Technol.* 102 (2003) 366.
- [26] Q. Wang, G. Wang, J. Jie, X. Han, B. Xu, J.G. Hou, *Thin Solid Films* 492 (2005) 61.
- [27] H.S. Kang, J.S. Kang, S.S. Pang, E.S. Shim, S.Y. Lee, *Mater. Sci. Eng., B, Solid-State Mater. Adv. Technol.* 102 (2003) 313.
- [28] A.V. Dijken, J. Makkinje, A. Meijerink, *J. Lumin.* 92 (2001) 323.
- [29] J. Bang, H. Yang, P.H. Holloway, *Nanotechnology* 17 (2006) 973.

## CURRICULUM VITAE

**Name** Mr. Wiradej Thongsuwan

**Date of Birth** May 20, 1978

**Education** B.S. (Physics), Chiang Mai University,  
Chiang Mai, 2000.  
M.S. (Applied Physics), Chiang Mai University,  
Chiang Mai, 2005.

**Scholarship** Ph.D. scholarship from the Ministry of University  
Affairs of Thailand.

### Publications

1. W. Thongsuwan, T. Kumpika, P. Singjai, "Photocatalytic property of colloidal TiO<sub>2</sub> nanoparticles prepared by sparking process "*Current Applied Physics*" **8**, 563-568 (2008).
2. W. Thongsuwan, S. Aukkaravittayapun, P. Singjai, "Preparation of Iron Oxide Nanoparticles by a Pyrosol Technique" *Key Engineering Materials* **353-358**, 2175-2178 (2007).

3. W. Thongsuwana, T. Kumpikaa, P. Thongmanee, S. Bovonsombut and P. Singjai, "Antibacterial activity of TiO<sub>2</sub> nanoparticles prepared by sparking process", *Under submission*.
4. T. Kumpika, W. Thongsuwan, P. Singjai, "Atomic force microscopy imaging of ZnO nanodots deposited on quartz by sparking off different tip shapes", *Surface Interface Analysis* **39**, 58- 63 (2007).
5. T. Kumpika, W. Thongsuwan, P. Singjai, "Optical and electrical properties of ZnO nanoparticle thin films deposited on quartz by sparking process" , *Thin Solid Films* **516**, 5640-5644 ( 2008).

#### Conference Participations:

1. W. Thongsuwan, S. Aukkaravittayapun, P. Singjai, "Preparation of Iron Oxide Nanoparticles by a Pyrosol Technique", *The 2006 Asian Pacific Conference for Fracture and Strength (APCFS'06)*, Sanya, Hainan Island, China. November 22-25, 2006.
2. W. Thongsuwan, T. Kumpika, P. Singjai, "Fabrication of TiO<sub>2</sub> nanoparticle thin films on glass by a novel sparking method", *The materials Tri-conference: The 5<sup>th</sup> MP3, Thin Films, ISAC – 3*, Singapore. December, 2006.